# A NOVEL HEAT SINK DESIGN AND NUMERICAL ANALYSIS OF HEAT TRANSFER ON THERMOELECTRIC GENERATOR SURFACES TO IMPROVE THERMOELECTRIC POWER GENERATION

**2023**
**MASTER THESIS**
**MECHANICAL ENGINEERING**

**Yasir Shakir ABDULSATTAR**

**Thesis Advisor**
**Assist. Prof. Dr. Enes KILINÇ**

# A NOVEL HEAT SINK DESIGN AND NUMERICAL ANALYSIS OF HEAT TRANSFER ON THERMOELECTRIC GENERATOR SURFACES TO IMPROVE THERMOELECTRIC POWER GENERATION

**Yasir Shakir ABDULSATTAR**

**Thesis Advisor**
**Assist. Prof. Dr. Enes KILINÇ**

**T.C.**
**Karabük University**
**Institute of Graduate Programs**
**Department of Mechanical Engineering**
**Prepared as**
**Master Thesis**

**KARABÜK**
**September 2023**

I certify that in my opinion, the thesis submitted by Yasir Shakir ABDULSATTAR titled "A NOVEL HEAT SINK DESIGN AND NUMERICAL ANALYSIS OF HEAT TRANSFER ON THERMOELECTRIC GENERATOR SURFACES TO IMPROVE THERMOELECTRIC POWER GENERATION" is fully adequate in scope and in quality as a thesis for the degree of Master of Science.

Assist. Prof. Dr. Enes KILINÇ .....
Thesis Advisor, Department of Mechanical Engineering

This thesis is accepted by the examining committee with a unanimous vote in the Department of Mechanical Engineering as a Master of Science thesis. Sep. 1, 2023

| Examining Committee Members (Institutions) | | Signature |
|---|---|---|
| Chairman | : Prof. Dr. Mehmet ÖZKAYMAK (KBU) | ..... |
| Member | : Assist. Prof. Dr. Enes KILINÇ (KBU) | ..... |
| Member | : Assist. Prof. Dr. Fatih UYSAL (SUBU) | ..... |

The degree of Master of Science by the thesis submitted is approved by the Administrative Board of the Institute of Graduate Programs, Karabuk University.

Assoc. Prof. Dr. Zeynep ÖZCAN .....
Director of the Institute of Graduate Programs

*"I declare that all the information within this thesis has been gathered and presented in accordance with academic regulations and ethical principles and I have according to the requirements of these regulations and principles cited all those which do not originate in this work as well."*

Yasir Shakir ABDULSATTAR

## ABSTRACT

**M. Sc. Thesis**

**A NOVEL HEAT SINK DESIGN AND NUMERICAL ANALYSIS OF HEAT TRANSFER ON THERMOELECTRIC GENERATOR SURFACES TO IMPROVE THERMOELECTRIC POWER GENERATION**

**Yasir Shakir ABDULSATTAR**

**Karabük University**
**Institute of Graduate Programs**
**Department of Mechanical Engineering**

**Thesis Advisor:**
**Assist. Prof. Dr. Enes KILINÇ**
**September 2023, 76 pages**

Waste heat recovery systems are very significant applications for reducing global warming and carbon dioxide gas emissions and reducing energy shortage crises. Such challenges lead researchers and scientists to develop and optimize these systems by recovering a huge amount of waste heat and to generate more electrical energy instead. In this study, thermoelectrical technology is utilized to develop a waste heat recovery system, since it uses a thermoelectric generating system which includes a thermoelectric generator (TEG) with two heat sinks that are embedded into hot and cold channels where hot exhaust gases are harvested to heat a TEG hot surface and cooling water is utilized to cool the cold surface. This is accomplished by establishing a three-dimensional model as a novel prototype that includes modern modifications within computational fluid dynamics (CFD). This research presents a novel heat sink design since the optimization on a square pin fin heat sink is achieved by changing the

cross-sectional area of the pins with a constant number of pins for the heat sink to obtain different horizontal and vertical gaps. This study attains three models (A, B and C) of heat sinks according to pin size such that the pins gradually increase in size from Model A to Model C. Novel physical parameters are considered, including inlet temperatures and inlet mass flow rates throughout the literature investigation.

The Reynolds number for hot exhaust gas is in the range of 4,457 to 14,246 and for cooling water 7,197. Exhaust gas temperatures are in the range of 403.15 K to 553.15 K, whereas the cooling water temperature is 303.15 K. Numerical analyses for these three models are performed and comparisons among them are carried out in terms of temperature distribution, heat transfer rates, pressure drop, output power and conversion efficiency. The results show that the optimal inlet mass flow rate and optimal inlet temperatures are 0.028 kg/s and 553.15 K to achieve the best performance. In addition, the temperature difference of 185.56 K is the best obtained difference in the present study. The heat transfer rates increase when the surface area of the square pins is increased, and the vertical and horizontal gaps decrease. Moreover, the highest heat transfer rate on the hot surface is 113.69 W. The best output power and conversion efficiency were up to 4.44 W and 3.903%, respectively, and all of these high findings occurred in Model C. It was also observed that the highest pressure drop and highest pumping power occurred in Model C, in which net output power decreased and was equivalent to 4.07 W. A parametric study was performed on Model C under different inlet temperatures and various mass flow rates.

**Keywords** : Thermoelectric generator, waste heat recovery (WHR), computational fluid dynamics (CFD), heat sink, fins.

**Science Code :** 91412

# ÖZET

**Yüksek Lisans Tezi**

**TERMOELEKTRİK GÜÇ ÜRETİMİNİN İYİLEŞTİRİLMESİ İÇİN YENİ BİR ISI KUYUSU TASARIMI VE TERMOELEKTRİK JENERATÖR YÜZEYLERİNDEKİ ISI TRANSFERİNİN SAYISAL ANALİZİ**

**Yasir Shakir ABDULSATTAR**

**Karabük Üniversitesi**
**Lisansüstü Eğitim Enstitüsü**
**Makine Mühendisliği Anabilim Dalı**

**Tez Danışmanı:**
**Dr. Öğr. Üyesi Enes KILINÇ**
**Eylül 2023, 76 sayfa**

Atık ısı geri kazanım sistemleri, küresel ısınma ve karbondioksit gazı emisyonlarının azaltılması ve enerji kıtlığı krizlerinin azaltılması için çok önemli uygulamalardır. Bu tür zorluklar, araştırmacıları ve bilim insanlarını büyük miktarda atık ısıyı geri kazanarak ve bunun yerine daha fazla elektrik enerjisi üreterek bu sistemleri geliştirmeye ve optimize etmeye yönlendirmektedir.

Bu çalışmada, bir atık ısı geri kazanım sisteminin geliştirilmesi için termoelektrik teknolojisi kullanılmıştır. Bunun için sıcak egzoz gazlarının sıcak yüzeyini ısıttığı ve soğuk yüzeyin soğutulması için soğutma suyunun kullanıldığı sıcak ve soğuk kanallara gömülü iki ısı kuyusuna sahip bir termoelektrik jeneratör (TEJ) sistemi kullanılmıştır. Hesaplamalı akışkanlar dinamiği (HAD) kullanılarak modern modifikasyonlar içeren üç boyutlu yeni bir model oluşturulmuştur. Bu modelde, farklı yatay ve dikey

boşlukların elde edilmesi için ısı kuyusunda kanatçık sayısı sabit tutularak kanatçıkların kesit alanı değiştirilmiş, kare kesitli kanatçığa sahip ısı kuyusu üzerinde optimizasyon gerçekleştirilerek yeni bir ısı kuyusu tasarımı yapılmıştır. Bu çalışmada, kanatçık boyutuna göre üç farklı modelde (A, B ve C) ısı kuyusu elde edilmiştir. Kanatçıların boyutu Model A'dan Model C'ye kademeli olarak artmaktadır.

Sıcak egzoz gazı için Reynolds sayısı 4.457 ile 14.246 aralığında değiştirilmiştir. Soğutma suyu için ise Reynolds sayısı 7.197'dir. Egzoz gazı sıcaklıkları 403.15 K ile 553.15 K aralığında iken soğutma suyu sıcaklığı 303.15 K'dir. Bu üç model için sayısal analizler gerçekleştirilmiş ve sıcaklık dağılımı, ısı transfer hızı, basınç düşüşü, çıkış gücü ve dönüşüm verimliliği açısından aralarında karşılaştırmalar yapılmıştır. Sonuçlar, en iyi performansı elde etmek için optimum giriş kütle akış hızının ve optimum giriş sıcaklıklarının 0,028 kg/s ve 553,15 K olduğunu göstermektedir. Ayrıca, 185,56 K sıcaklık farkı bu çalışmada elde edilen en iyi sıcaklık farkıdır. Kare kanatçıkların yüzey alanı artırıldığında ve dikey ve yatay boşluklar azaldığında ısı transfer oranları artmaktadır. En iyi çıkış gücü ve dönüşüm verimi sırasıyla 4,44 W ve %3,903'e kadar çıkmış ve bu yüksek bulguların tümü Model C için gerçekleşmiştir. Ayrıca, en yüksek basınç düşüşünün ve en yüksek pompalama gücünün, net çıkış gücünün azaldığı ve 4,07 W'a eşdeğer olduğu Model C'de meydana geldiği gözlemlenmiştir. Farklı giriş sıcaklıkları ve çeşitli kütle akış hızları altında Model C üzerinde parametrik bir çalışma yapılmıştır.

**Anahtar Kelimeler :** Termoelektrik jeneratör, atık ısı geri kazanımı, hesaplamalı akışkanlar dinamiği, ısı kuyusu, kanat tasarımı.

**Bilim Kodu :** 91412

**ACKNOWLEDGEMENT**

Firstly, it is pleasing to express my sincere thanks and appreciation to my dear supervisor Assist. Prof. Dr. Enes KILINÇ for his valuable support and advice. I would like to thank Prof. Dr. Kamil ARSLAN for advising me since his office was always open whenever I ran into a trouble spot or had a question during my study journey. My thanks also go to all my professors who taught me throughout this journey, including Prof. Dr. Engin GEDİK for advising me during my thesis study.

I must especially express my profound gratitude to my parents, my brother Dr. Sarmid and my sister for providing me with continuous support and helpful encouragement throughout my study years. Also, my uncle, Prof. Dr. Mahmoud R. AL-Qaissy, motivated me to complete my postgraduate study and supported me through my bachelor study; for this I am truly grateful. This accomplishment would not have been possible without any of them. Thank you.

**CONTENTS**

**Page**

APPROVAL ..... ii
ABSTRACT ..... iv
ÖZET ..... vi
ACKNOWLEDGEMENT ..... viii
CONTENTS ..... ix
LIST OF FIGURES ..... xi
LIST OF TABLES ..... xiii
SYMBOLS AND ABBREVITIONS ..... xiv

PART 1 ..... 1
INTRODUCTION ..... 1
1.1. ENERGY ..... 1
1.2. THERMOELECTRIC ENERGY ..... 2
1.3. HEAT SINKS ..... 5
1.3.1. Plate Fins ..... 6
1.3.2. Pin Fins ..... 6
1.4. THERMOELECTRIC EFFICIENCY ..... 7
1.5. THERMOELECTRIC APPLICATIONS ..... 9
1.6. THESIS PLAN ..... 12

PART 2 ..... 13
2.2. ORIGINALITY OF THE STUDY ..... 20
2.3. OBJECTIVES OF THE STUDY ..... 21

PART 3 ..... 23
METHODOLOGY ..... 23
3.1. PHYSICAL CONFIGURATION ..... 23
3.2. MATHEMATICAL FORMULATIONS ..... 28

**Page**

3.2.1. Governing Equations and Operating Parameters ..... 29
3.2.2. Thermoelectric Module ..... 32
3.3. NUMERICAL ANALYSIS ..... 36
3.3.1. Numerical Analysis Stages ..... 36
3.3.2. Numerical Method ..... 42
3.3.3. Turbulent Model Validation ..... 43
3.3.4. Model Grid Independence ..... 44
3.4. BOUNDARY CONDITIONS ..... 47

PART 4 ..... 48
4.1. TEMPERATURE DISTRIBUTION ..... 48
4.2. HEAT TRANSFER RATE ..... 56
4.3. PERFORMANCE OF THE THERMOELECTRIC MODULE ..... 58
4.4. EFFECT OF DIFFERENT TEMPERATURES UNDER THE VARIOUS MASS FLOW RATES ..... 63
4.5. PRESSURE DROP AND NET OUTPUT POWER ..... 66

PART 5 ..... 69
CONCLUSIONS AND SUGGESTIONS ..... 69

REFERENCES ..... 71

RESUME ..... 76

## LIST OF FIGURES

**Page**


Figure 1.1. Schematic illustration of a TEG ..... 3
Figure 1.2. Schematic illustration of a TEC ..... 3
Figure 1.3. Thermoelectric module ..... 4
Figure 1.4. Thermoelectric generating system. ..... 4
Figure 1.5. Schematic diagram of a plate fin heat sink ..... 6
Figure 1.6. Schematic diagram of a square pin fin heat sink ..... 7
Figure 1.7. Typical TE efficiencies for various ZT values ..... 8
Figure 1.8. Constructions of AETEGs: (a) cooling by liquid, (b) cooling by air, (c) construction of a TEG ..... 10
Figure 3.1. Configuration of the entire model. ..... 24
Figure 3.2. Illustration of the opening location. ..... 24
Figure 3.3. Configuration of Model A. ..... 25
Figure 3.4. Configuration of Model B. ..... 26
Figure 3.5. Configuration of Model C. ..... 26
Figure 3.6. Compact thermoelectric generating system modelled in this study. ..... 28
Figure 3.7. Three-dimensional model. ..... 36
Figure 3.8. Common types of mesh. ..... 37
Figure 3.9. Boundary layers in turbulent flow. ..... 38
Figure 3.10. Difference between experimental and CFD curves. ..... 39
Figure 3.11. Height of the first layer. ..... 40
Figure 3.12. Cross-section of the meshed model. ..... 41
Figure 3.13. Illustration of inflation layers. ..... 41
Figure 3.14. Flow chart of calculation procedures. ..... 43
Figure 3.14. Temperature differences in the first model (A). ..... 46
Figure 3.15. Temperature differences in the second model (B). ..... 46
Figure 3.16. Temperature differences in the third model (C). ..... 47
Figure 4.1. Relationship between inlet temperature and temperature difference. ..... 49
Figure 4.2. Relationship between inlet mass flow rate and temperature difference. ..... 49

**Page**

Figure 4.3. Isothermal contour for the upper surface of the hot channel in Model A. ..... 50
Figure 4.4. Isothermal contour for the upper surface of the hot channel in Model B..... 51
Figure 4.5. Isothermal contour for the upper surface of the hot channel in Model C..... 51
Figure 4.6. Isothermal contour of a square pin fin heat sink in Model A. ..... 52
Figure 4.7. Isothermal contour of a square pin fin heat sink in Model B..... 53
Figure 4.8. Isothermal contour of a square pin fin heat sink in Model C..... 53
Figure 4.9. Isothermal contours of the hot surface of the TEG for the three models. ..... 54
Figure 4.10. Isothermal contours of the cold surface of the TEG for the three models. ..... 55
Figure 4.11. Comparison of the three models in terms of temperature differences... 55
Figure 4.12. Relationship between temperature differences and heat transfer rates.. 56
Figure 4.13. Relationship between mass flow rates and heat transfer rates..... 57
Figure 4.14. Comparison among the three models in terms of heat transfer rates..... 58
Figure 4.15. Comparison among the three models in terms of surface areas. ..... 58
Figure 4.16. Relationship between temperature differences and output power..... 59
Figure 4.17. Relationship between temperature difference and efficiency..... 60
Figure 4.18. Relationship between mass flow rate and output power. ..... 61
Figure 4.19. Relationship between mass flow rate and efficiency..... 61
Figure 4.20. Comparison among the three models in terms of output power..... 62
Figure 4.21. Comparison among the three models in terms of efficiency. ..... 62
Figure 4.22. Comparison of heat transfer rate under different temperatures and different mass flow rate conditions. ..... 64
Figure 4.23. Comparisons of temperature differences under different temperatures and different mass flow rate conditions. ..... 65
Figure 4.24. Comparisons of output power under different temperatures and different mass flow rate conditions..... 66
Figure 4.25. Comparisons of conversion efficiency under different temperatures and different mass flow rate conditions. ..... 66
Figure 4.26. Comparison among the three models in terms of pressure drop. ..... 67
Figure 4.27. Comparison among the three models in terms of output power versus net output power. ..... 68

## LIST OF TABLES

**Page**

Table 3.1. Square pin fin models with their dimensions. ..... 25
Table 3.2. Properties of TE materials, fluids and heat sink materials. ..... 27
Table 3.3. Novel temperatures used in the numerical analyses. ..... 31
Table 3.4. Velocities and mass flow rates for hot and cold fluids. ..... 32
Table 3.5. Element sizes for whole bodies. ..... 38
Table 3.6. Grid independence for the first model (A). ..... 44
Table 3.7. Grid independence for the second model (B). ..... 45
Table 3.8. Grid independence for the third model (C). ..... 45
Table 4.1. Different types of fins added to thermoelectric generator systems from the previous literature. ..... 63

## SYMBOLS AND ABBREVITIONS

### SYMBOLS

| | |
|---|---|
| $T$ | : Temperature |
| $\dot{m}$ | : Mass flow rate |
| $dT$ | : Temperature difference |
| $dV$ | : Voltage difference |
| $\beta$ | : Thomson effect |
| $q$ | : Reversible heat |
| $I$ | : Electrical current |
| $zT$ | : Figure of merit |
| $\sigma$ | : Electrical conductivity |
| $K$ | : Thermal conductivity |
| $\eta_{max}$ | : Maximum efficiency of TEG |
| $T_H$ | : Hot surface temperature |
| $T_C$ | : Cold surface temperature |
| $COP_{max}$ | : Radiation heat transfer |
| $Re$ | : Reynolds number |
| $L$ | : Length |
| $W$ | : Width |
| $H$ | : Height |
| $\rho$ | : Density |
| $V$ | : Flow velocity |
| $D$ | : Hydraulic diameter of channels |
| $\mu$ | : Dynamic viscosity of fluids |
| $\nabla$ | : Mathematical operator |
| $P$ | : Pressure |
| $C_p$ | : Specific heat at constant pressure |

| | |
|---|---|
| t | : Time |
| $S_g$ | : Source term in energy equation |
| $(k)$ | : Turbulence kinetic energy |
| $\varepsilon$ | : Dissipation rate |
| $\mu_t$ | : Turbulent (or eddy) viscosity |
| $\sigma_k$ | : Turbulent Prandtl numbers for ($k$) |
| $\sigma_\varepsilon$ | : Turbulent Prandtl numbers for ε |
| $\dot{Q}_{in}$ | : Heat transfer rate input |
| $\dot{W}_{out}$ | : Output work |
| $\dot{g}$ | : Power generation per unit volume |
| $\rho_{TE}$ | : Thermoelectric material's density |
| $C$ | : Specific heat capacity of thermoelectric module |
| $S$ | : Seebeck coefficient |
| $R_{TE}$ | : Resistance of thermoelectric module |
| $R_{external}$ | : Resistance of external load |
| $\forall$ | : Volume of thermoelectric module |
| $p$ | : Electrical resistivity |
| $A$ | : Area |
| $C_1$, $C_2$ | : constants |
| $P_{out}$ | : Output power of thermoelectric module |
| $\dot{q}$ | : Heat flux |
| $q$ | : Generated reversible heat |
| $\eta$ | : Efficiency |
| $\dot{Q}$ | : Heat transfer rate |
| $\Delta P$ | : Pressure drop |
| $P_{Pump}$ | : Pumping power |
| $P_{Net}$ | : Net output power |
| $\dot{V}$ | : Volumetric flow rate |

## ABBREVIATIONS

| | |
|---|---|
| *WHR* | : Waste heat recovery |
| *CFD* | : Computational fluid dynamics |
| *TE* | : Thermoelectric |
| *PE* | : Pyroelectric |
| *TEG* | : Thermoelectric generator |
| TEJ | : Termoelektrik jeneratör |
| *TEC* | : Thermoelectric cooler |
| *RTG* | : Radioisotope thermoelectric generator |
| *AETEGs* | : Automotive exhaust thermoelectric generating systems |
| *HS* | : Hot state |
| HAD | : Hesaplamalı akışkanlar dinamiği |
| *CS* | : Cold state |
| *COP* | : Coefficient of performance |

# PART 1

# INTRODUCTION

## 1.1. ENERGY

Energy is the fundamental source converted by our daily life processes, expanding from the residential to industrial sectors, including food as the basic source of energy for our physiological activities. There are many resources of energy, such as coal, crude oil, natural gas, hydroelectricity, nuclear, and renewables.

In terms of the ecological impact of energy resource exploitation, there are many issues about which researchers should concerned, including the cost of extraction, ability to transform, distribution through utility grids, demand for power, and a consciousness regarding energy utilization and consumption. All the issues above are significant and need to be taken into consideration by all countries around the world. The consumption of energy has been increasing since the beginning of the first industrial era in 1840, which is considered a perfect index to the maturity of the economy [1].

The environmental pollution and energy shortage crises have had a negative effect on all countries worldwide in terms of global warming and carbon dioxide gas emissions, which are an important part of the environmental problems which should be solved. Developed industries are now considered a significant challenge since the impact directly affects our environment by generating a huge amount of waste heat. Waste heat is classified generally into three main categories based on temperature limitations, including low level waste heat below 230°C, medium level waste heat is in the range of 230°C to 650°C, and high level waste heat at temperatures higher than 650°C. To decrease the negative impacts and reduce environmental problems, there are significant approaches to recover and utilize waste heat by using a waste heat recovery system (WHR). This strategy relies on unoccupied energy (heat energy which exits to

the atmosphere) and simply converts it to another form of energy by using many advanced technologies [2].

## 1.2. THERMOELECTRIC ENERGY

Nowadays, there are serious concerns about emissions and reducing them, which leads us to waste heat recovery and energy transformations by using the current modern technologies that can be divided into thermodynamic approaches and cross-thermal effects such as thermoelectric (TE) devices and pyroelectric (PE) devices [2]. The phenomenon of the thermoelectric module was discovered in the 18th century, when the researchers connected two different metals and produced a temperature difference (dT) which resulted in an electrical current or electromotive force. This generated current or electromotive force is called the Seebeck effect and is mainly indicated by thermoelectric generators (TEGs), as shown in Figure 1.1. The Seebeck coefficient is a property-based constant and is different for various materials. It has a low value for metals at about 0 μV/K, but it has greater values for semiconductor materials at about 200 μV/K. The Seebeck coefficient ($S$) is defined as:

$$S = \frac{dV}{dT} \tag{1.1}$$

where the temperature difference (dT) is directly proportional to the voltage difference of the two metals (dV). It was found that the various conducting materials absorb or reject the heat at the joints, depending on the current direction in the circuit. This state is called the Peltier effect and mainly occurs in thermoelectric coolers (TECs), as shown in Figure 1.2.

Another effect which is considered integrated into the Peltier effect is the Thomson effect, which is the rate of generated reversible heat due to the current in the single conductor. It is defined as:

$$\beta = \frac{q}{I.dT} \tag{1.2}$$

where $\beta$ is the Thomson effect coefficient in V/K, q is the generated reversible heat, I is the current in amperes, and dT is the temperature difference in Kelvin [3].

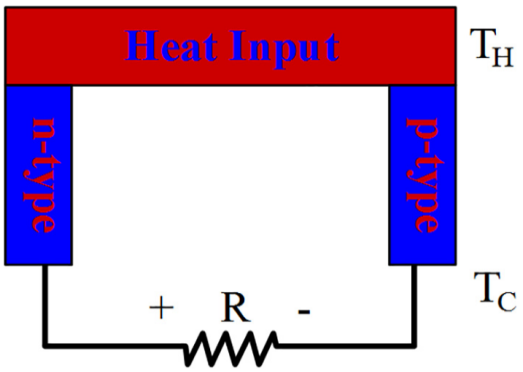


Figure 1.1. Schematic illustration of a TEG [4].

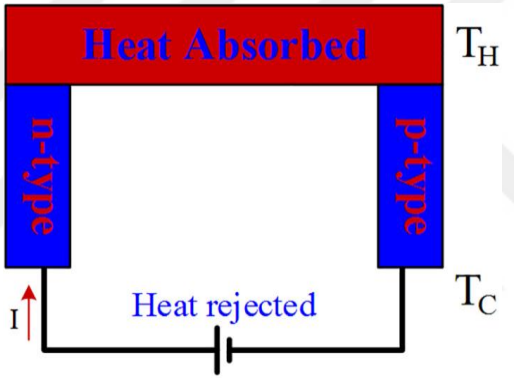


Figure 1.2. Schematic illustration of a TEC [4].

In general, thermoelectric technology is categorized into TEGs and TECs. TEG modules are specific power generation engines and mainly flat structures which are composed of many thermoelements or legs (P and N types), these legs are connected in a series pattern electrically by conductive tabs and in a parallel pattern thermally, placed between two ceramics plates (Figure 1.3). Thermoelectric generating systems consist of three main components, namely TEGs, heat and cold sources are transmitted using fluid, and a heat sink that transfers heat between TEGs and sources to maximize heat transfer [5].

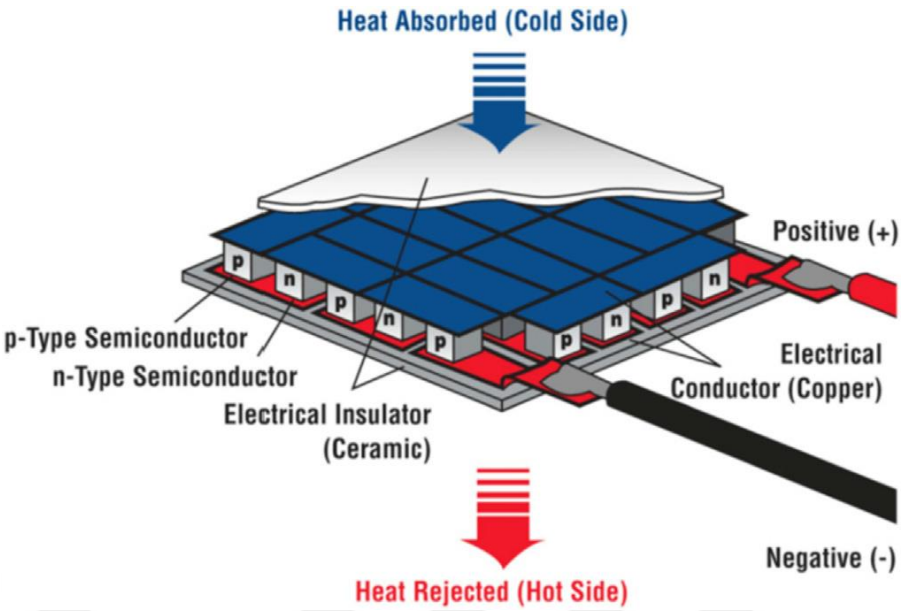


Figure 1.3. Thermoelectric module [6].

The main components of the thermoelectric generating system (Figure 1.4):

- The core of this system is formed by TEGs.
- Heat and cold sources are transported using fluids.
- Heat sinks transfer heat between TEGs and sources to maximize heat transfer [5].

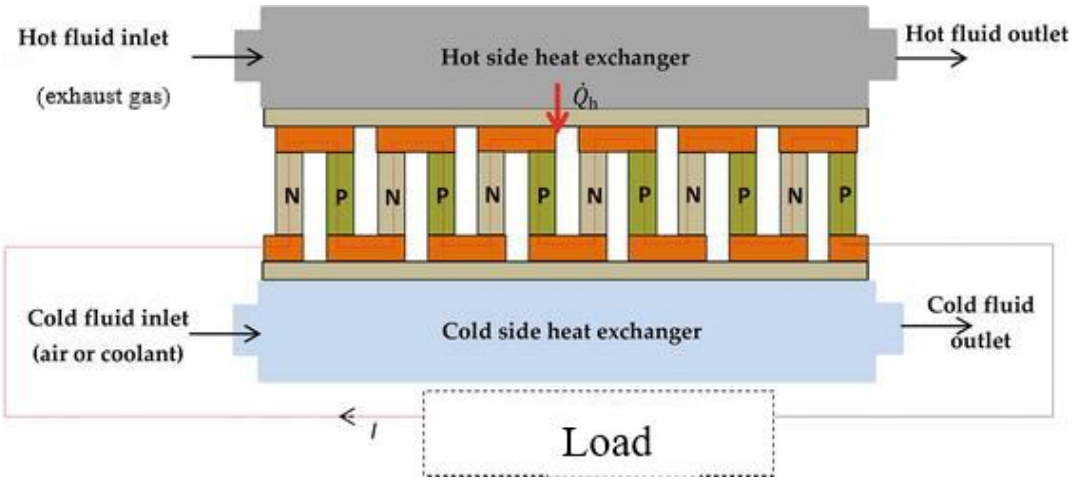


Figure 1.4. Thermoelectric generating system.

## 1.3. HEAT SINKS

A heat sink is a device that is attached to advanced electronic elements to dissipate the heat generated from these elements while operating, such as thermoelectric generators, processors of laptops or integrated circuit elements in general. There are two processes to describe how a heat sink performs. The first of which is where the heat is transferred by a conduction process between the hot surface of an electronic element like a TEG and the surface of a heat sink that is fixed onto the surface of the element. The second process is convection between the heat sink and its surroundings that can be classed into two methods:

- **Passive Method**

This method includes geometrical modifications to the flow passage by interrupting or changing the existing flow behavior. In this method, the heat transfer coefficient is developed and the pressure drop is increased. Extended surfaces such as fins are used to improve the transfer of heat between the main surface (heat sink's base) and the surrounding fluid. These are considered examples of passive methods, so the free convection process is depended upon here.

- **Active Method**

This is not a simple cooling method as it depends on a forced convection process which requires extra input power to operate the device with fans or pumps to increase the rate of heat transfer by modifying the flow parameters like pressures and velocities. Nevertheless, it is a common method and currently has been found in many applications.

There are many techniques for increasing the rate of heat transfer by increasing the temperature differences between the models and its surroundings, improving the convection heat transfer coefficient, or extending the surface area of heat sink. The main objective when manufacturing fins is currently to reduce their cost and size. Many procedures should be taken into consideration when optimizing fins by changing

their size and geometrical shapes. The fluid flow pattern will therefore be changed in addition to their performance parameters, heat transfer rate, and pressure drop. There are different types of fins, but the most well-known fins are plate fins, cylindrical pin fins, and square pin fins, which are used to improve thermoelectric generator applications [7].

### 1.3.1. Plate Fins

Plate fin heat sinks are a variety of heat sink that are commonly used where efficient heat dissipation is required. They consist of a limited number of flat fins that are perpendicular to the base of heat sink. All of these fins have constant thickness and height, are extended longitudinally according to the side length of the base, as shown in Figure 1.6, thereby providing a larger surface area and better dissipation. However, dissipation of heat to ambient fluid would be better. The heat sink is made of highly conductive materials such as copper or aluminium according to need. These have a number of advantages, such as easy machining, a simple structure, low cost. However, they do not have the better results in performance evaluations [8].

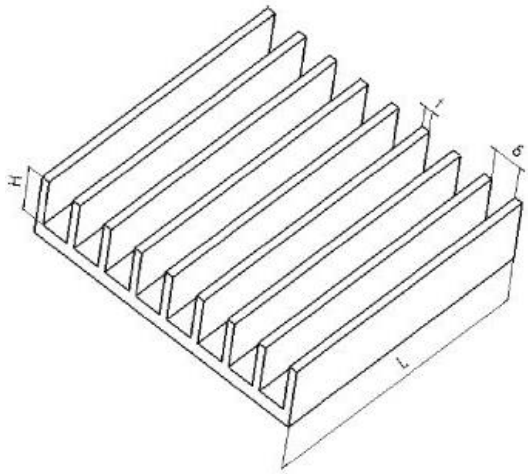


Figure 1.5. Schematic diagram of a plate fin heat sink [8].

### 1.3.2. Pin Fins

It is a type of heat sink that is also commonly utilized. It consists of a base and fins, but it is unlike the previous type (plate fin). The fins grow from the base as pins and

are distributed in a specific uniform pattern (as in an array). The heat transfer is improved by increasing the heat sink's surface area as the number of pins increases. The design of this type gives users the largest exposed surface area and many gaps in two dimensions since the spaces between the pins (gaps) permit the passage of an ideal amount of fluid. High conductivity materials can be employed in the manufacturing of this type. The pin fin heat sinks are considered more efficient than the plate fin type, and has high thermal performance. However, it is more expensive and more complicated to manufacture.

There are many types of heat sink which are classified according to pin shape, including cylindrical, square (Figure 1.7), and rectangular [9].

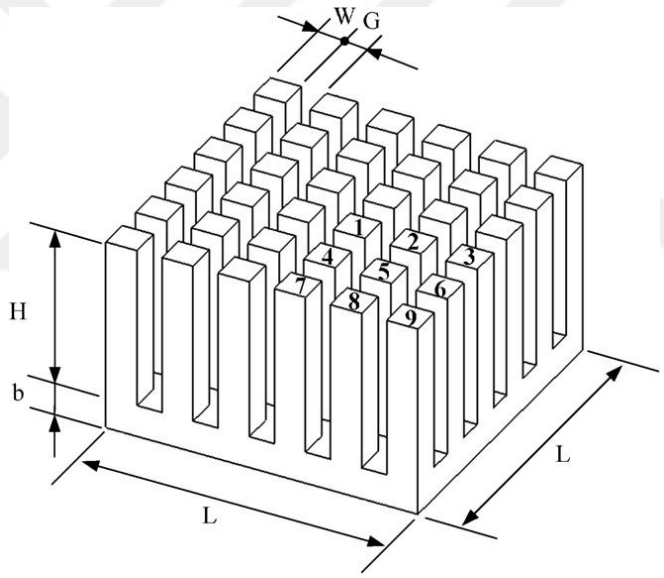


Figure 1.6. Schematic diagram of a square pin fin heat sink [9].

## 1.4. THERMOELECTRIC EFFICIENCY

The efficiency of TE material is an important issue on which researchers are working in order to develop and improve the TE module's performance. To specify the thermoelectric performance of certain materials, we use a dimensionless parameter, known as figure of merit (zT), which is the production of the z factor (i.e., the factor of merit of TE materials) and T, the average temperature. This is defined as:

$$zT = \frac{S^2}{K}\sigma T \tag{1.3}$$

Where K and σ represent the electrical and thermal conductivities of materials, respectively. Figure of merit is considered the best way to compare the properties of materials for materials manufacture. Moreover, it is an important parameter in power maximizing issues. In recent years, the famous material, which is utilized in the manufacturing of TE modules, is bismuth telluride ($Bi_2Te_3$), which has a figure of merit value in the range of 0.5 to 1. Currently, there are expectations of developments of material to have a TE of over average the value of $zT = 1$ as the efficiency of TE is currently about 5%. Some laboratories are working to develop this value to ZT = 2, which means the efficiency of TE is equal to approximately 10%, as shown in Figure 1.5.

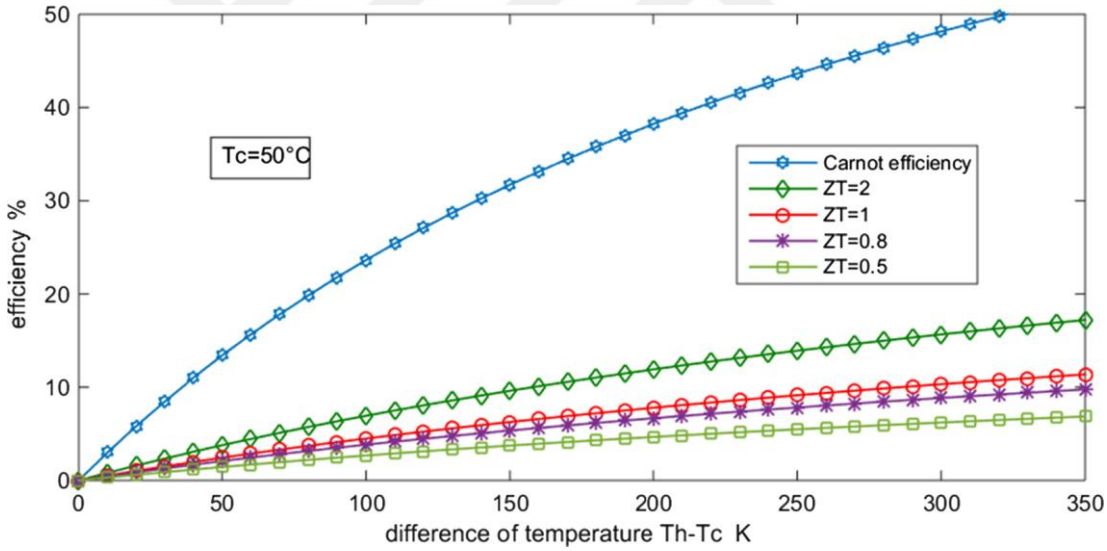


Figure 1.7. Typical TE efficiencies for various ZT values [10].

The ratio of electrical energy generated ($W_{elec}$) to thermal energy absorbed by the hot surface of a thermoelectric module, defines the maximum efficiency of TEGs, which for a maximum electric load is stated by the following relationship:

$$\eta_{max} = \frac{W_{elec}}{Q_H} = \frac{T_H - T_C}{T_H} x \frac{\sqrt{1 + \overline{ZT}} - 1}{\sqrt{1 + \overline{ZT}} + \frac{T_C}{T_H}} \tag{1.4}$$

where $T_H$ is the temperature of the hot surface of the TE module, $T_C$ the temperature of the cold surface of the module, and $dT = T_H - T_C$ the temperature difference. Z is the factor of merit of the TE modules.

While TECs are used for cooling purposes only by submitting to the input voltage, the performance of TECs is evaluated by the maximum coefficient of performance (COP) equation as follows [3][10]:

$$COP_{max} = \frac{T_c}{T_H - T_c} x \frac{\sqrt{1 + \overline{ZT}} - \frac{T_c}{T_H}}{\sqrt{1 + \overline{ZT}} + 1} \tag{1.5}$$

## 1.5. THERMOELECTRIC APPLICATIONS

TEG has many advantages including its utility to convert thermal energy into electricity directly without passing through the processes of heat engines. It also has a long lifespan and does not need maintenance. It is a simple solid module that has no moving parts nor uses working fluids. Moreover, its operation is noiseless, so utilization of TEG becomes possible in any working condition without any gas emissions. Moreover, it is environmentally friendly [10].

There are many applications, such as in the aerospace industry, in which researchers use TEGs in different ways, including radioisotope thermoelectric generators (RTGs) which depend on heat generated by plutonium-238's natural radioactive decay. RTGs are utilized based on their low weight and high reliability, especially when sunlight is insufficient to operate solar panels since the solar radiation on the earth is 1,375 $W/m^2$, while at Pluto, it is approximately 1 $W/m^2$. Moreover, RTGs are compact, continuously operational and highly reliable devices to generate electricity during space explorations.

The second application is utilized in remote areas due to minimal maintenance and high reliability. TEGs are used on gas pipelines, wellheads, offshore platforms,

telecommunications sites and for security surveillance. These modules utilize the produced heat by the burning of fuel or natural gases. To optimize the efficiency of heat transfer process, the burner heats one side of the TE module and natural convection cools the other side using a heat sink.

The third application pertains to the waste heat field. The main challenge facing humanity now is the increase in greenhouse gas emissions and its ecological impact. Therefore, researchers endeavor to reduce the environmental effects by recovering waste heat energy produced by various industries and converting that waste heat into electrical energy. The transportation sector would probably find the use of thermoelectric technology the most attractive sector because of automobiles, aircraft, and ships use combustion engines. For example, the consumption of energy in a gasoline-powered automobile is detailed as follows: 25% for engine operation, 30% for engine cooling system, 5% for additional losses, and 40% exits as exhaust gas. For diesel light and duty trucks in which full consumption is supposed to be 100 kW of fuel power, the power of 30 kW represents the heat losses through exhaust gases. If the heat loss is converted into electricity even at an efficiency of 3%, the electrical power will be 900 watts, these findings were presented by Fiat Research Centre. Figure 1.6 shows the construction of an automotive exhaust thermoelectric generating system (AETEG) [11].

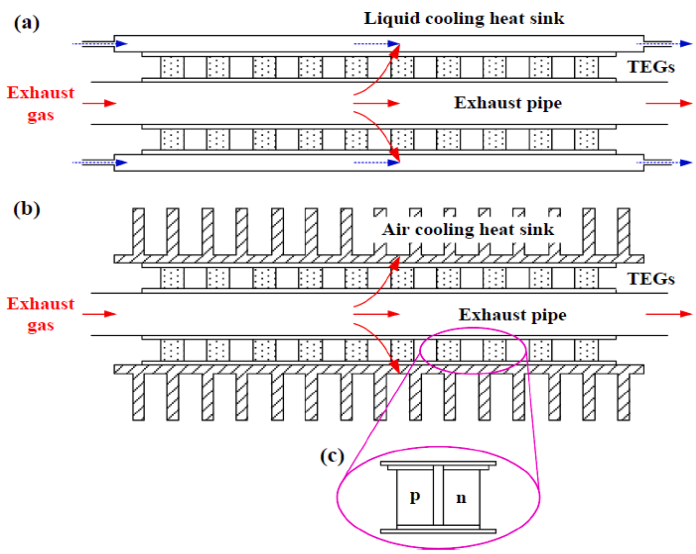


Figure 1.8. Constructions of AETEGs: (a) cooling by liquid, (b) cooling by air, (c) construction of a TEG [11].

Another side of the waste heat field is industry, where most of the time exhaust gas heat is discharged by chimneys into the atmosphere. However, there are different applications which can reuse the waste heat to convert it to electrical energy through various thermodynamics cycles and thermoelectric technologies [12]. For example, in 2009 [13], a Japanese company began to test thermoelectric generating systems at a carburizing furnace of a power plant. This plant works by burning gas containing chemical particles such as CO, $H_2$ and $N_2$. They produced 20 kW of power by burning the gas to heat the hot surfaces of the module. TEG modules were sixteen and made of $Bi_2Te_3$ materials. Additionally, the heat exchanger collected 20% of the heat (4 kW). The researchers found that the efficiency and electrical output power of thermogenerating system were 5% and 214 W respectively during the test.

The utilization of TEG in the microelectronics field is possible, especially with advanced sensors in various factories to improve the quality of products and reduce the time of production. These sensors need a few hundred microwatts or a few milliwatts to operate instead of empowering through long cables or from batteries which are difficult and costly. Manufacturers seek a simple microgenerator to make sensors autonomous. However, there are many heat sources in factories from different processes. TEGs may be a permanent solution for sensors wherever low maintenance is not necessary. These modules have a long lifespan, are simple units (only a few square millimeters), and require little power. Nowadays, wireless application use is increasing widely and the consumption power of microcontrollers, actuators and sensors are reduced by applying advanced electronics technology, resulting in the future development and utilization of micro-TEGs [10].

In addition to waste heat recovery applications, researchers utilize TEG with photovoltaic solar panels to use the sun’s heat by attaching a number of TEGs onto the back of panels so that power can be generated from TEG. The efficiency of this hybrid system is better than those of individual systems.

## 1.6. THESIS PLAN

This study consists of five main parts. An introduction and theoretical background of thermoelectric generating systems which consist of thermoelectric energy and applications as well as the efficiency estimation are detailed. Additionally, heat sink types and their advantages are presented in Part 1. In Part 2, the originality of the thesis is clarified and a comprehensive literature review and the novelty of heat sink design and their parameters are presented. Part 3 includes physical configurations, the novel heat sink design and novel inlet parameters as well as mathematical formulations, boundary conditions and numerical analysis stages. In addition, the turbulent model validation and grid independence test are presented in a detailed manner in this part. The results and isothermal contours of different cases of numerical analysis are illustrated and discussions and comparisons among different models are presented in Part 4. Finally, the conclusion and suggestions for further studies are given in Part 5.

# PART 2

# LITERATURE REVIEW

## 2.1. LITERATURE REVIEW

According to the field of research, there have already been classifications of thermoelectric devices in terms of their features; therefore, thermoelectric generators or coolers have been adopted into many scientific articles. In our literature survey, the search process depends on the five factors to study the scientific articles. The first is the type of thermoelectric module. The heat sink classification is the second, including the plate fin, square pin fin, cylindrical pin fin, etc. Geometry and number of fins is the third factor, the inlet temperatures of the hot and cold fluid are the fourth, and the final factor is the state of flow as to whether it is turbulent or laminar according to specific Reynolds numbers. Reviews of previous studies mostly focus on the effect of fluid properties of the heat exchange process in heat sinks integrated with thermoelectric generators in terms of output power and conversion efficiency of thermoelectric generating systems.

Chen et al. [14] studied the improvement of heat transfer performance of a TEG with two kinds of heatsinks: plate fins and also square pin fins in terms of output power, temperature distribution and conversion efficiencies. Heat sinks were fixed onto the hot surface of a TEG inside a hot channel. The three-dimensional model embedded two channels, hot flue gas (automotive exhaust gas) would flow through a hot channel while cooling water would flow through a cold channel, and the comparison was achieved among three cases, namely those without fins, those with plate fins (a fixed number of fins), and those with square pin fins (with different numbers of fins), Moreover, this study developed a compromised approach to obtain the best point in terms of materials cost and heat transfer rate. The study was performed using CFD software with results revealing that Over a plate heat sink, a square pin fin heat sink is

better. The best square pin number is 78, which compared to the plate-fin heat sink, increases output power by 24.14%, whereas according to compromise method, the best number of fins is 54.

Chiou et al. [15] studied TE system performance and industrial low-temperature waste heat fields by developing a compact model combining thermoelectric generators, computational fluid dynamics and plate fin heat sinks. There are three issues related to this study, the first being when the thermoelectric module was divided into two, four, or eight partitions to examine the module's performance in comparison to the thermoelectric module without division, the findings suggested that there is no difference between a partitioned module and complete module with regard to output power and conversion efficiency. The second issue was found in the investigation of four combinations (of working fluids) in a counter flow pattern. The first combination was that of hot and cold fluid being hot waste water and cooling water, the second where the hot and cold fluid were hot waste water and cooling air, the third being that of exhaust gas with cooling water, and the fourth being that of hot gas with cooling air. The study found that hot wastewater combined with cooling water is more efficient than the other combinations. The third issue was when utilizing three thermoelectric generators and plate fin heat sinks in a different number of fins with a range of 0-27, the evaluation was carried out using three Reynolds numbers (10, 100 and 1000). The findings showed that the best fins number at Re = 10 and Re = 100 was 21, while it was 27 at Re = 1000, and that a higher number of fins would increase the output power and efficiency by 105.5% and 43.94%, respectively.

Jie Liu et al. [16] studied waste heat recovery systems in casting metals industries. The researchers used a system consisting of 576 TEGs exposed to flue gas by using different heat sinks such as plate fins, square pin fins, and cylindrical pin fins while conducting numerical analyses. A thermoelectric system was subjected to impinging flow (heat flow along pin height), and comparisons among heat sinks showed that when the lower inlet velocities of 4-5 m/s occurred, the plate fin heat sinks were optimum than the other kinds of heat sink and that the cylindrical pin fin heat sinks presented the optimal heat transfer performance when the inlet velocity was higher than 5 m/s.

Şara [17] performed an experimental study to investigate the heat transfer, friction losses and performance parameters on a staggered square pin fins attached to a flat plate as a base with different lengths, embedded into a rectangular duct by taking into consideration the effect of the clearance ratio, which is the ratio of the gap between the tip of the fin height and the duct channel to fin height, as well as the ratio (interfering ratio) between fin spacing to the thickness of the fin with different numbers of pin fins. Flow was turbulent, with Reynolds numbers in the range of 10,000 to 34,000. The results revealed that pin fins enhance heat transfer compared not having pin fins. According to this study, friction loss also increased when the clearance and interfering ratios dropped. To improve thermal performance, the clearance and interfering ratios should be lower.

Yang et al. [18] accomplished a comparative study on square, cylindrical and elliptical pin fin heat sinks. The performance of the heat transfer was investigated, and the inline and staggered configurations of the fins were examined. The study suggests that an increase in fin density generally intensifies the heat transfer coefficients for all types of pin fins.

Delfani et al. [19] utilized thermoelectric technology in impressed current cathodic protection systems for gas pipelines in remote areas by using four thermoelectric generators with a plate-fin heat sink for each module. The waste heat of combusted gas which was extracted from the pipeline was utilized to generate a voltage difference and output power. The findings indicated that a larger temperature difference can produce a higher voltage as a directly proportional relationship, while indicating an inverse effect of heat sink thermal resistance in return for voltage difference.

Wang et al. [20] optimized the performance of a thermoelectric generating system in two stages of optimization by utilizing two methods, namely an analytical method to present heat transfer of plate fin heat sink, and a numerical method to investigate the performance of the system. The first stage comprised optimal gaps being specified according to an analytical method, and in the second stage (compromise programming), the fins size was optimized by decreasing the length of the plate fin and increasing the frontal area of the heat sink. The results suggested that the output

power density increases by 88.7% and the conversion efficiency decreases by 20.93% according to the compromise point.

Rezania et al. [21] performed a comparative study between a plate fin heat sink and a cross-cut heat sink to improve the performance of thermoelectric generators over a wide range of inlet velocities (in laminar flows). For the reduction of the required cooling power and increasing TEG output power, various temperatures and thermal conductivities of semiconductors were applied during calculations, all of which showed that When using the plate fin heat sink at lower inlet velocities, the highest net output power value is generated, whereas in cases of utilizing a cross-cut heat sink, the maximum net output power would be achieved at higher inlet velocities.

A finned tubular thermoelectric generator was developed by Zoui et al. [5] for gas and liquid pipeline applications to recover waste heat extracted from pipes during hot water flows. This module was manufactured by using an annular fin heat sink and quadratic profiled legs sorted axially. The performance of the annular heat sink and thermal resistance properties were investigated numerically using computational fluid dynamics software. The simulations suggested that the best efficiency occurs when there were 2-3 mm gaps between the fins and the height of fins were 11-13 mm.

Liu et al. [22] developed a radiative cooling heat sink to improve heat transfers from the cold side of a thermoelectric generator by investigating its convective and radiative cooling. They found that the negative factors on power generation were atmospheric humidity and ambient temperature, while the positive factors included the wind speed and heater temperature. The radiative cooling heat sink was compared to the aluminium heat sink. The study found that the output power with a radiative cooling heat sink is 32% higher than that with the aluminium heat sink.

Tzeng et al. [23] performed a parametric study on a thermoelectric system integrated with a heat absorber on the hot surface and a heat sink on the cold surface by using the forced convection technique. The heat sink and heat absorber consisted of pin fins arranged as an array. The experiments were set up by supposing internal heat

generation and the Seebeck effect at various inlet conditions to achieve optimal heat transfer performance in terms of inlet temperature and mass flow rate.

Kim et al. [24] performed a comparative study among plate fin and pin fin heat sinks according to be subjected to impinging flow experimentally in terms of various flow rates and channel widths. The proposed model was extracted from experiments to obtain pressure drops and thermal resistance for the heat sinks. The findings indicate that the pin-fin heat sink has a lower thermal resistance than the plate-fin heat sink under low dimensionless pumping power and a large length of the heat sink, while the pin-fin heat sink possesses a higher thermal resistance than the plate-fin heat sink under high dimensionless pumping power and a small length of the heat sink.

Rosendahl et al. [25] proposed and implemented a three-dimensional model in CFD for TEG legs to study the temperature distribution on the semiconductors of a thermoelectric module and to evaluate the produced current. This proposed model was considered to be reliable for all temperatures with dependent characteristics of the materials as well as including different effects such as multiphysical coupled and nonlinear fluid thermal electric. To predict and improve system performance, the thermoelectric model can be integrated with multiple CFD models of heat sources as a continuum domain.

Chen et al. [26] analyzed the thermal stresses in thermoelectric generator components by establishing a three-dimensional model of a waste heat recovery system and utilizing various square pin fins on the hot surface since the increase in the number of fins increases the heat transfer rate on the hot surface, while the temperature distribution is different according to heat transfer rate. However, they found that maximum thermal stress occurred in the legs of the corners of the module and it was direct proportional to the output power. As a result, the reduction of the thickness of the ceramic plate and legs of the module caused lower thermal stresses in the thermoelectric module.

Jang et al. [27] investigated a compact three-dimensional model consisting of a thermoelectric generator module embedded in chimney walls and attached to a plate

fin heat sink on the hot side inside the chimney channel to recover waste heat. The radiation effect was considered, and the cold side of the thermoelectric generator was exposed to cooling water and attached to a plate. The inlet velocities and inlet temperatures of the hot fluid (flue gas) were investigated. The height of the fins and the number of fins was examined throughout this model. The results showed that the increase in fin height and the number of fins increase the output power, conversion efficiency, pressure drop and pumping power density.

Wan et al. [28] embedded a thermoelectric generator in an automotive exhaust system consisting of a thermoelectric module attached to a plate-fin heat sink, catalytic converter and muffler. Different materials of plate-fin were examined, such as steel, copper and aluminium. They found that when the thermal conductivity was high, the surface temperature and output power would increase accordingly, and that the development of an integrated automotive thermoelectric generator system would improve the noise reduction of the exhaust system and increase the efficiency of a thermoelectric generator.

Ma et al. [29] studied the impact of longitudinal vortex generators (by considering them as a plate fin heat sink) on the thermoelectric generator performance inside a channel with laminar flow. The Seebeck, Peltier, Thomson and Joule heating effects were considered, and thermal and electrical properties were included in a numerical analysis which indicated that the longitudinal vortex generators would produce vortices through channel sections thereby improving the thermal and electrical performance of the thermoelectric generator. As a comparison with a smooth channel without vortices, the input heat and voltage were increased by 41-75%. With a high Reynolds number, the heat input and pressure drop with vortices were much larger than those without vortices. When the hot side inlet temperature increases, the input heat and voltage also increase, but the cold side has a simple effect.

Luo et al. [30] improved the heat transfer performance on the hot side of a heat exchanger in a converging thermoelectric generator system including a converging heat exchanger design. The utilization model of numerical analysis was multiphysical fluid-thermoelectric coupled field to perform an exact, comprehensive numerical

analysis. A comparison between converging and conventional thermoelectric generator systems was conducted, and it was found that the output power of the converging system was 5.9% higher than that of the conventional system. In the converging system, when the air temperature is high, the output power increases. However, the increase in air mass flow rate in a range of 5-60 g/s causes a reduction in output power. The experimental study was carried out and compared to the numerical study, which was found to be in good agreement.

Cao et al. [31] studied the insertion of a heat pipe into an integrated automotive exhaust system with thermoelectric generators for waste heat recovery. To enhance the heat transfer rate, an experimental model was configured to achieve an optimal inclination angle of the heat pipe and the best insertion depth. The researchers discovered that the optimal insertion depth and angle were 60 mm and 15°, respectively. By comparing between automotive exhaust systems with and without heat pipes, it was shown that the optimized open circuit voltage and maximum output power were higher than that without heat pipes. It was also observed that the generation system efficiency was improved by increasing the exhaust temperature. Furthermore, the highest pressure drop with fins was higher by two times without fins. Elankovan et al. [32] examined different thermal system configurations including parallel flow, counter flow and constant fluid temperature. The cold side of a heat sink exposed to the ambient environment to evaluate the performance of a thermoelectric generator system in a flue gas channel considering the variable length of the hot channel. The researchers investigated fin parameters such as the number of fins, fin height and fin spacing (gaps). The comparison was carried out among different configurations, and the results revealed that the best efficiency and output power were in a constant fluid temperature configuration. However, through temperature drops along the channel, the greatest output power and conversion efficiency were 172.34 kW and 4.3%, respectively, for the cold heat sink exposed to the ambient environment when compared to parallel and counter flow thermal system configurations.

Yüncü et al. [33] performed an experimental study of natural convection heat transfer by utilizing a plate-fin heat sink and horizontal base. The fin parameters, such as fin

height, spacing of fins and base to ambient temperature differences, were investigated. While the number of fins, fin thickness and fin length were constant, the findings showed that the rise in temperature difference increases the heat transfer rate. The optimum fin spacing is not influenced much on the temperature differences. The researchers also discovered that there is suitable fin spacing for every fin height, and that the heat transfer rate depends strongly on the fin spacing to fin height ratio and the number of fins.

## 2.2. ORIGINALITY OF THE STUDY

The motivation of this study is to recover waste heat instead of having it dissipate by converting it into electrical energy and removing any negative environmental impacts by utilizing the TEG system with two heat sinks. The study develops a novel heat sink design to maximize output power and efficiency by improving the performance of the thermoelectric generating system. In addition, it analyzes and investigates the effects of the inlet mass flow rates of hot and cold fluid and inlet temperatures on pressure drop, output power and conversion efficiency.

Square pin fin heat sinks, among various kinds of fins, are appropriate for low level waste heat recovery because they have been shown a good heat exchange performance due to previous studies. Moreover, CFD is a common, efficient and reliable tool for predicting the performance of thermoelectric generating systems.
In the present thesis, the aim of study is to construct a three-dimensional model as a novel prototype (TEG with two heat sinks) which includes modern modifications on the shape of a square pin fin's geometry. The number of fins is constant and the surface area of the pins is changed to form three models regarding the same fin's arrangement; however, it means that the spacing between the pins is a variable parameter. Most scientific studies, however, focus on the changing of the number of fins to increase the heat exchange area.

A review of previous research shows that few studies suggest combining two heat sinks, one combination of which are on the hot side and the other on the cold side of TEG in a thermoelectric generating system. Therefore, a physical parameter

investigation is performed for both heat sinks in this study with a hot inlet temperature in the range of 403.15 K to 553.15 K and inlet mass flow rates ranging from 0.0088 kg/s to 0.028 kg/s. A numerical analysis between different inlet hot temperatures and various mass flow rates is applied on the novel models.

By combining the CFD with the TEG system, the simulation and optimization of thermoelectric generation system performance and the heat transfer on both surfaces of TEG are achieved. The results are obtained through numerical analysis and are compared with those of existing geometries in the previous literature as validation. A comparison among the three models is carried out in terms of different findings. TEG is embedded into hot and cold channels to increase heat transfer and waste heat harvesting. Therefore, the fluid temperature and mass flow rates are investigated to obtain optimum results for output power, conversion efficiency and net output power (including pumping power). As a result, by using TEG technology, this study will reduce global warming and produce electrical energy from waste heat.

## 2.3. OBJECTIVES OF THE STUDY

A huge amount of waste heat is emitted from factories. This badly affects our environment. Therefore, we have studied and investigated the major advantages of waste heat by developing a thermoelectric generating system. Within this scope, in this study, a novel fin geometry for a heat sink has been designed and numerically investigated to enhance heat transfer on the hot and cold sides of a TEG. Within this regard, the following objectives have been achieved through this thesis:

- A novel design of fin geometry of the heat sink.
- A numerical investigation of the effects of fin geometry, Reynolds number, and fluid temperatures on the heat transfer as well as a study of the heat transfer on the hot and cold sides of a TEG.
- Evaluation of the output power and conversion efficiency of a TEG according to thermal contours of heat sinks and temperature distribution of square pin fins for three different models.

- The enhancement of a waste heat recovery system using modern modifications on a thermoelectric generating system.
- Waste heat recovery systems to achieve carbon dioxide emissions reduction and to contribute to reducing global warming.

# PART 3

# METHODOLOGY

The objectives of this part entail how to accomplish this study, including methods and materials and the presentation of a physical configuration of the model, the properties of a thermoelectric generator, hot and cold fluid specifications, and the mathematical formulations of all convection and conduction heat transfer processes and fluid flows. The numerical analysis is explained in parallel flow into the hot and cold channels. This part provides an investigative study of the numerical analysis on the thermoelectric surfaces, including temperature differences, heat flux and heat transfer rates. The geometry of the heat sink was designed by the CFD commercial software ANSYS DesignModeler 2020R2. The meshing and numerical simulations were solved using ANSYS Fluent 2020R2. The grid independence test was achieved in different cases, and assumptions and boundary conditions are also presented.

## 3.1. PHYSICAL CONFIGURATION

In this study, three variant geometries of square pin fin heat sinks are inserted inside hot and cold channels by penetrating an opening according to the heat sink's area to obtain a higher temperature difference between the hot and cold surfaces of the TEG for power generation. The whole configuration of study consists of a hot channel filled with waste heat exhaust gas, also a cold channel filled with cooling water and a thermoelectric generating system (including the TEG and two heat sinks). Both channels are made of aluminium. These channels are rectangular shaped, with (length × width × height) dimensions of 200 mm × 84 mm × 54 mm and a channel thickness of approximately 2 mm [14] (Figure 3.1). The thickness of the base of the heat sinks is equal to the thickness of the channels. The thickness of the opening into the channel wall is 2 mm (Figure 3.2).

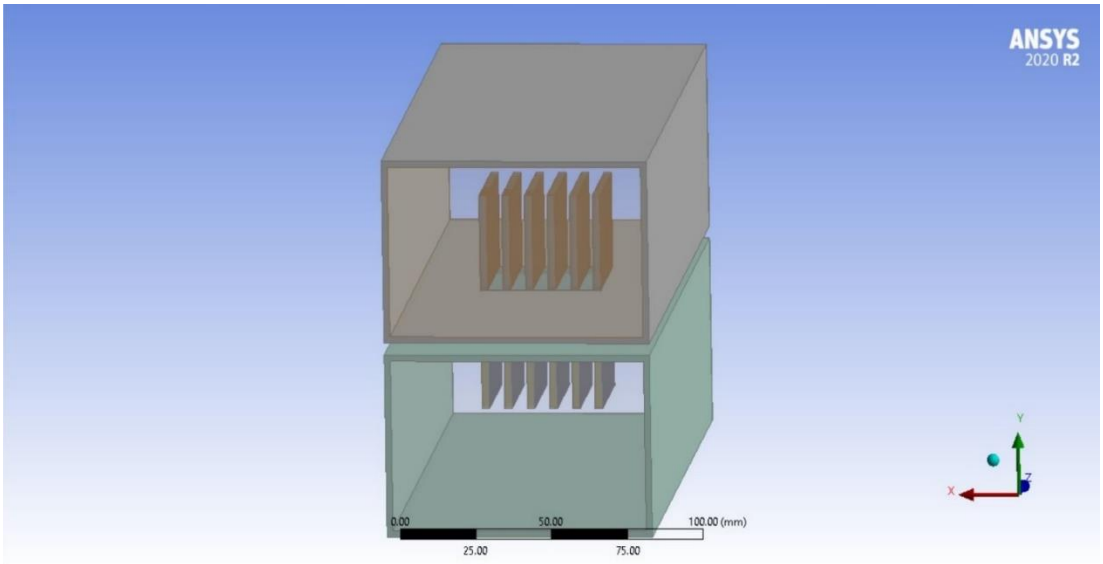


Figure 3.1. Configuration of the entire model.

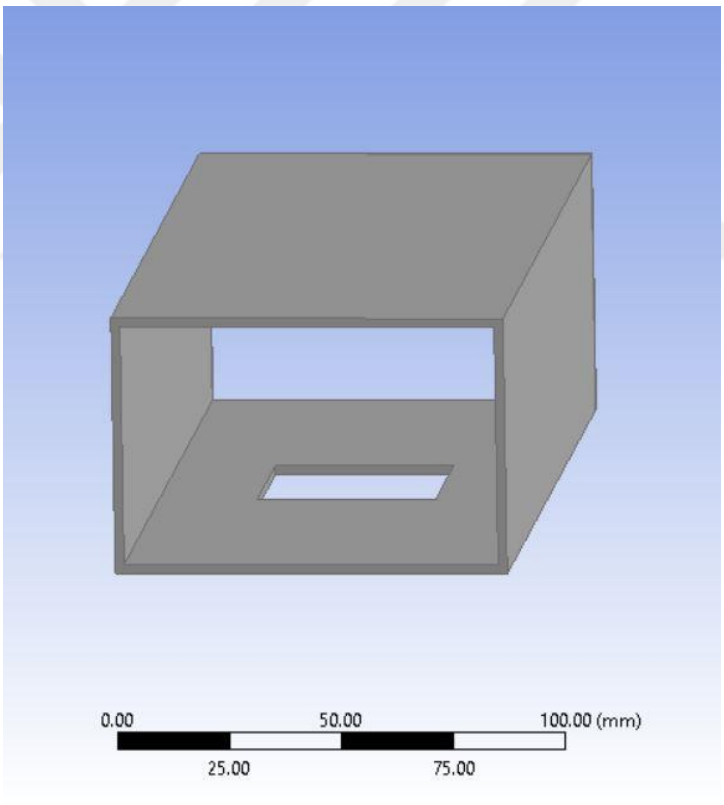


Figure 3.2. Illustration of the opening location.

Based on investigative studies and literature reviews, it can be shown that the best performance of the square pin fin heat sink occurs with 78 fins and a pin size of 2.5 mm × 2.5 mm × 30 mm (length × width × height) and when the pins are staggered in straight rows and columns [14]. It is therefore suitable to obtain novel geometries

of heat sinks in a variety of sizes and shapes. This study focuses on the square pin fin heat sink and optimizes the square pin at a constant height, thereby obtaining three different cross-sectional areas of the square pin. The horizontal and vertical gaps (distance between pins) also differ according to the model. In our study, there are three heat sink models (A, B and C), as shown in Table 3.1.

Table 3.1. Square pin fin models with their dimensions.

| **Model symbol** | **Size (L × W × H) (mm)** | **Vertical gaps (mm)** | **Horizontal gaps (mm)** | **Surface Area of fins ($mm^2$)** |
|---|---|---|---|---|
| **A** | 1.5 × 1.5 × 30 | 1.708 | 6.2 | 14,040 |
| **B** | 2 × 2 × 30 | 1.166 | 5.6 | 18,750 |
| **C** | 2.5 × 2.5 × 30 | 0.625 | 5 | 23,400 |

The arrangement pattern of the square pins is straight rows or columns in a 13 × 6 (row × column) configuration, which was taken from previous literature. The side of six pins faces the flow direction in each channel and the other side is located next to the flow. The horizontal gaps are arrayed, as shown in Figures 3.3 to 3.5.

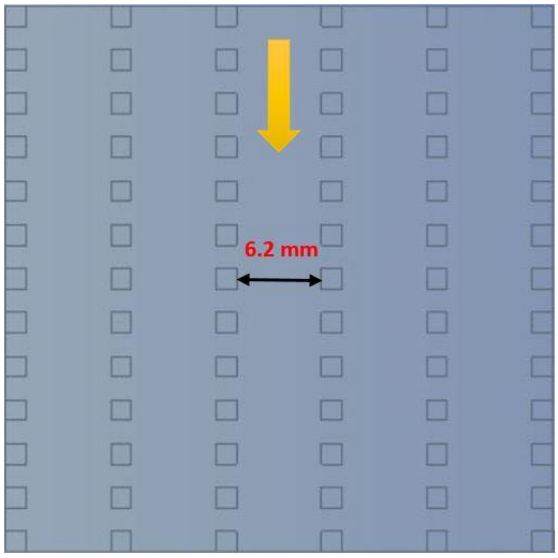


Figure 3.3. Configuration of Model A.

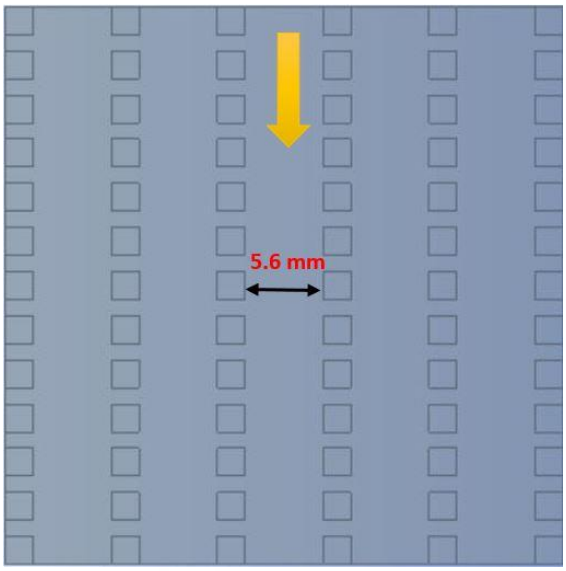


Figure 3.4. Configuration of Model B.

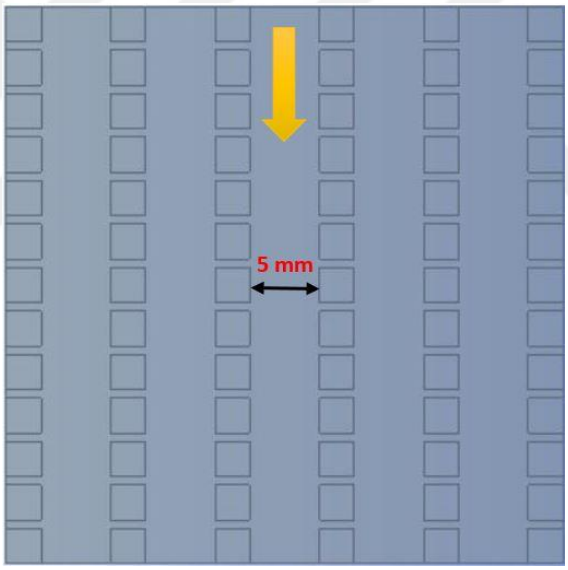


Figure 3.5. Configuration of Model C.

The commercial thermoelectric module (TEC1-12706) was utilized for this simulation since the module has 127 pairs of legs (P-type and N-type). These legs are made from semiconductors (bismuth telluride). This type of thermoelectric module is used at low and medium temperature conditions. The dimensions of the module (length × width × height) are 40 mm × 40 mm × 3.75 mm, with a leg length of 1.6 mm and cross-sectional area of 1.4 mm × 1.4 mm [25]. The heat sinks and channels are made of aluminium alloy, and their properties, specifications of TE material and fluid properties are mentioned in Table 3.2.

Table 3.2. Properties of TE materials, fluids and heat sink materials.

| Parameters | Units | Values |
|---|---|---|
| **TEG material** | | |
| Seebeck coefficient for P and N | V/K | **$226.8 \times 10^{-6}$** |
| Thermal conductivity | W/m.K | **1.52** |
| Electrical resistivity | Ω.m | **$1.447 \times 10^{-5}$** |
| | | |
| **Hot fluid (exhaust gas)** | | |
| Density | $kg/m^3$ | **0.644** |
| Specific heat at constant pressure | J/kg.K | **1045** |
| Thermal conductivity | W/m.K | **0.0444** |
| Dynamic viscosity | kg/m.s. | **$2.85 \times 10^{-5}$** |
| | | |
| **Cold fluid (cooling water)** | | |
| Density | $kg/m^3$ | **998.2** |
| Specific heat at constant pressure | J/kg.K | **4182** |
| Thermal conductivity | W/m.K | **0.6** |
| Dynamic viscosity | kg/m.s. | **0.001003** |
| | | |
| **Heat sink and channels material (aluminium alloy)** | | |
| Density | $kg/m^3$ | **2719** |
| Specific heat at constant pressure | J/kg.K | **871** |
| Thermal conductivity | W/m.K | **202.4** |

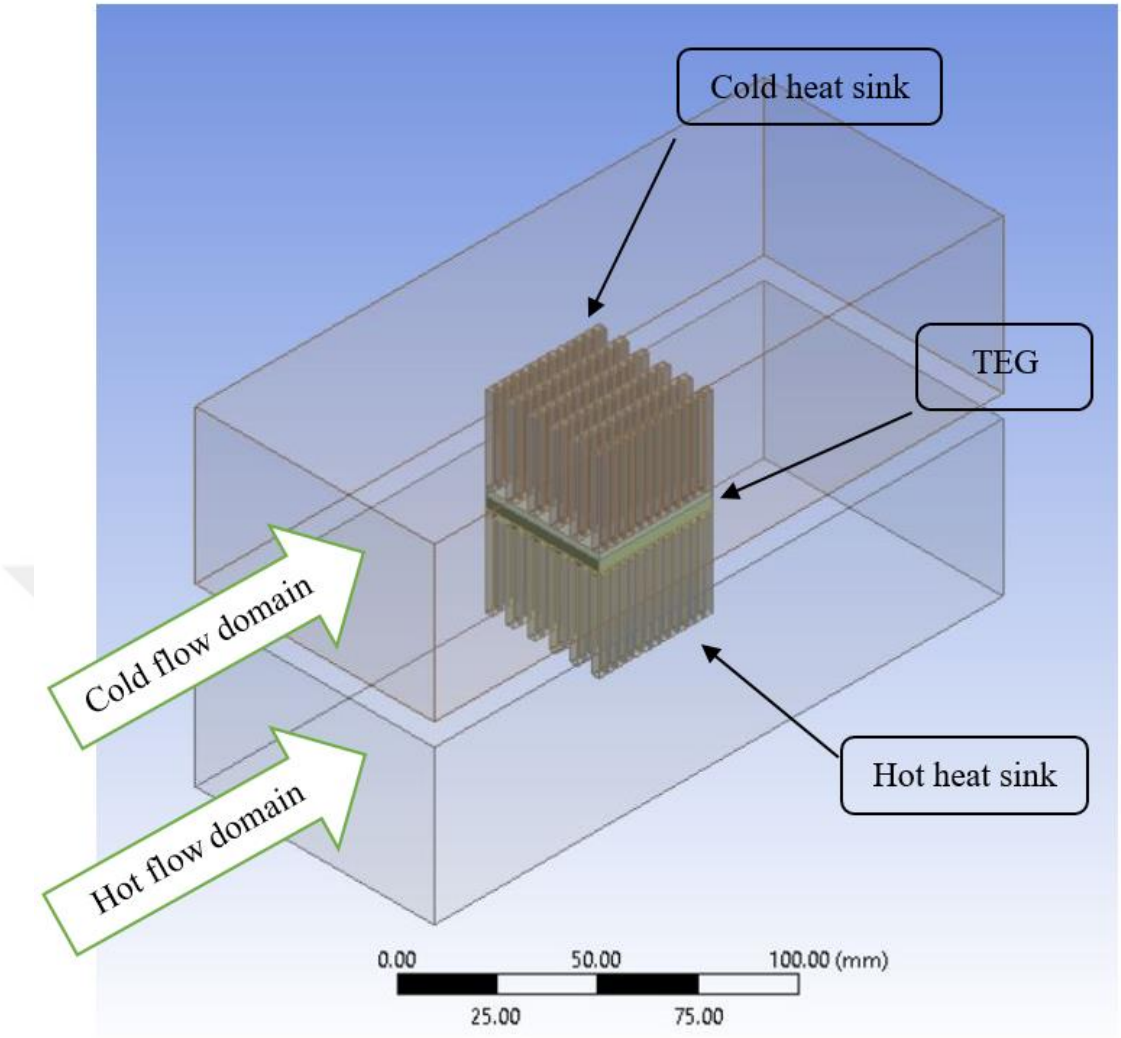


Figure 3.6. Compact thermoelectric generating system modelled in this study.

Figure 3.6 illustrates the compact thermoelectric generating system modelled in this study. The optimal configuration of models depends on output power and conversion efficiency results.

## 3.2. MATHEMATICAL FORMULATIONS

This section contains governing equations including (flow and energy fields) and thermoelectric generator relationships.

### 3.2.1. Governing Equations and Operating Parameters

To study flow through channels, there are specified assumptions that should be considered in order to apply flow and energy equations, including continuity, conservation of momentum (Navier-Stokes equation of motion) and the conservation of energy. The conventional utilization of the continuity and momentum equations is to find the velocity of a fluid at any point in a channel, while the energy equation is used to find the temperature at any point of the flow or on a surface, thereby making it easy to obtain heat flux and heat transfer rates. Convection is classified as a forced pattern because fluid motion is generated mechanically using pumping force since flow is assumed to be incompressible and at a steady state. The fluid must be in a continuum and Newtonian, with the properties of the fluid, such as thermal conductivity, dynamic viscosity and specific heat at constant pressure, having to be constant. The radiation and thermal stress between materials are ignored. The Reynolds number and aforementioned equations are defined below.

- Reynolds number equation:

$$Re = \frac{\rho V D}{\mu} \tag{3.1}$$

- Mass conservation equation (continuity equation):

$$\nabla . \vec{V} = 0 \tag{3.2}$$

- Momentum conservation equation:

$$\rho \frac{D\vec{V}}{Dt} = \rho \vec{g} - \nabla \vec{P} + \mu . \nabla^2 \vec{V} \tag{3.3}$$

- Energy conservation equation:

$$\nabla (\vec{V}.\rho.C_p.T) = \nabla \cdot (k \nabla T) + S_g \tag{3.4}$$

where ρ is the density of the fluid, V is the fluid velocity, D is the hydraulic diameter of the channels, P is the pressure of flow, $\mu$ and K refer to the dynamic viscosity and

thermal conductivity of the fluid, t is the time which refers to the state of flow, g is the gravitational acceleration, $C_p$ represents the specific heat at constant pressure, and $S_g$ is the source term.

The flow in the hot and cold channels is turbulent since the Reynolds number ranges between 4,457 and 14,246 for the hot fluid and is 7,197 for cold fluid. Therefore, in order to solve the two equations, the models of the ANSYS Fluent solver which are more suitable for turbulent flow are the K-ε model or the K-ω model. The Realizable K-ε model with enhanced wall treatment is utilized [34] in this study. The fluent software recommends utilization of the Realizable K-ε model over the others due to its more accurate predictions [35]. The equations of the turbulence model are defined below.

- Turbulence kinetic energy, (k):

$$\partial/\partial x_i\,(\rho k u_i) = \partial/\partial x_j\,[(\mu + \mu_t/\sigma_k)\,\partial k/\partial x_j] + G_k + G_b - \rho\varepsilon - YM + S_k \tag{3.5}$$

- Dissipation rate, ε:

$$\partial/\partial t\,(\rho\varepsilon) + \partial/\partial x_j\,(\rho\varepsilon u_j) = \partial/\partial x_j\,[(\mu + \mu_t/\sigma_\varepsilon)\,\partial\varepsilon/\partial x_j] + \rho C_1 S_\varepsilon - \rho C_2.\frac{\varepsilon^2}{K + \sqrt{v\varepsilon}} + C_{1\varepsilon}.\varepsilon/k.C_{3\varepsilon}G_b + S_\varepsilon \tag{3.6}$$

The turbulence kinetic energy K equation in the realizable K-ε model is the same as in the standard model, but the dissipation rate ε equation is different. $G_k$ and $G_b$ refer to the generation of turbulent kinetic energy due to mean velocity gradients and buoyancy, YM defines the contribution of the fluctuating dilatation in compressible turbulence to the overall dissipation rate, and $C_2$ and $C_{1\varepsilon}$ are constants. $\sigma_k$ and $\sigma_\varepsilon$ are the turbulent Prandtl numbers for k and ε respectively. $S_k$ and $S_\varepsilon$ are user-defined source terms. $\mu_t = \rho C_\mu.k^2/\varepsilon$, $C_{1\varepsilon} = 1.44$, $C_2 = 1.9$, $\sigma_k = 1.0$, and $\sigma_\varepsilon = 1.2$ [36].

This study suggests novel parameters, such as three velocities of hot inlet fluid and three inlet temperatures. The fourth velocity and temperature are from a previous study. Table 3.3 shows the four temperatures for hot fluid and one for cold fluid.

Table 3.3. Novel temperatures used in the numerical analyses.

| Fluid temperatures | |
|---|---|
| **For exhaust gas (hot fluid) in Kelvin** | |
| 1 | **403.15** |
| 2 | **453.15** |
| 3 | **503.15** |
| 4 | **553.15** |
| **For cooling water (cold fluid) in Kelvin** | |
| Constant temperature | **303.15** |

To find the Reynolds number, the hydraulic diameter of channels is first to be determined:

$$\text{Diameter}_{\text{hydraulic}} = \frac{4 \times \text{Area}}{(2 \times \text{W}) + (2X\text{H})}$$

$$\text{Diameter}_{\text{hydraulic}} = 0.06574 \text{ m}$$

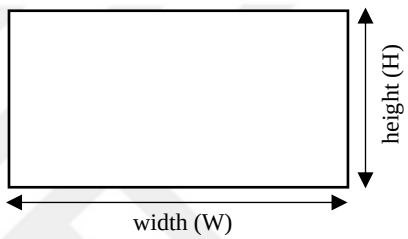


Then by applying the Reynolds number equation (3.1),

At a low velocity of 3 m/s, the Reynolds number equals 4,457. For the second velocity of 5 m/s, the Reynolds number equals 7,427. For the third velocity of 7.5 m/s, the Reynolds number equals 11,141. For the final velocity of 9.59 m/s, the Reynolds number equals 14,246, as shown in Table 3.4.

To find mass flow rates for every suggested velocity, we should apply a one-dimensional flow rate equation:

$$\dot{m} = \rho . \text{V} . \text{A}$$

The mass flow rates are derived from the one-dimensional flow rate equation, as shown in Table 3.4.

Table 3.4. Velocities and mass flow rates for hot and cold fluids.

| Velocity (m/s) | Mass flow rates (kg/s) | Reynolds number |
|---|---|---|
| | **For exhaust gas (hot fluid)** | |
| 3 | 0.0088 | **4,457** |
| 5 | 0.0146 | **7,427** |
| 7.5 | 0.0219 | **11,141** |
| 9.59 | 0.028 | **14,246** |
| | | |
| | **For cooling water (cold fluid)** | |
| 0.11 | 0.5 | **7,197** |

### 3.2.2. Thermoelectric Module

The objective of using a thermoelectric generator is to recover waste heat discharged into the environment and generate electrical power instead. In the current study, a thermoelectric module is considered to be a source term unit. It is necessary to identify the equations that are regarded with the source term, namely those of output power and efficiency. The First Law of Thermodynamics is used to derive the heat equation in the TEG's control volume, as follows:

$$\Sigma\dot{Q}_{in} - \Sigma\dot{W}_{out} + \dot{E}_g = \dot{E}_{st} \tag{3.7}$$

where $\dot{E}_g$ is the produced energy rate per unit volume of the TEG, and $\dot{E}_{st}$ the stored energy rate or depository rate. They are defined thus:

$$\dot{E}_g = \dot{g}.\,dx.\,dy.\,dz \tag{3.8}$$

$$\dot{E}_{st} = \rho_{TE}\,C\,\frac{\partial\overline{T}}{\partial t}.dx.dy.dz \tag{3.9}$$

where $\rho_{TE}$ and C refer to the thermoelectric material's density and its corresponding specific heat capacity. A source term involved in a control volume system is proposed for this study. Due to the First Law of Thermodynamics, the heat equation is defined as:

$$(\dot{q}_x - \dot{q}_{x+dx})\, dy.dz + (\dot{q}_y - \dot{q}_{y+dy})\, dx.dz + (\dot{q}_z - \dot{q}_{z+dz})\, dx.dy + \dot{E}_g = \dot{E}_{st} \tag{3.10}$$

where $\dot{q}$ is the heat flux. Equations 3.8 and 3.9 and the conduction equation = $-K\nabla T$ must be substituted into Equation 3.10, and by dividing the overall equation by the volume (dx.dy.dz), we have the following:

$$\partial/\partial x(k.\partial T/\partial x) + \partial/\partial y(k.\partial T/\partial y) + \partial/\partial z(k.\partial T/\partial z) + \dot{g} = 0 \tag{3.11}$$

where K refers to the thermal conductivity of a thermoelectric material and $\dot{g}$ is the source term, which means the power generation per module volume in order to the self-consistency theory [37].

Thermoelectric materials possess constant properties. Moreover, the Thomson effect is neglected, and as a result, a temperature gradient is generated by the average temperature difference between the hot and cold surfaces of the TEG, which subsequently induces current, thus [38]:

$$I = (S\Delta T)/(R_{TE} + R_{external}) \tag{3.12}$$

where S is the Seebeck coefficient (since $S = S_p = S_n$), and $R_{TE}$ and $R_{external}$ are the thermoelectric module and external load resistances, respectively.

The produced electrical power of thermoelectric module is determined by the following equation [39]:

$$P_{out} = I^2.\, R_{external} = [(S\Delta T)\ /\ (R_{TE} + R_{external})]^2.\, R_{external} \tag{3.13}$$

To find the maximum power of the thermoelectric module, the research [40] considered module's resistance to be equivalent to external load resistance, such as in independence matching.

$$R_{TE} = R_{external} \tag{3.14}$$

By substituting Equation 3.14 into Equation 3.13, we get the maximum output power equation [41], thus:

$$\text{Maximum power} = S^2.\ \Delta T^2/4R \tag{3.15}$$

The source term $\dot{g}$, which equals Sg in energy Equation 3.4, is the thermoelectric module's maximum output power per module volume at a specific temperature difference, and it is presented as follows:

$$\dot{g} = -\ (S^2.\ \Delta T^2/4R)\ /\ \forall \tag{3.16}$$

where $\forall$ is the volume of the thermoelectric module. The source term $\dot{g}$ has a negative sign, while it is necessary to find module resistance by depending on the aforementioned resistivity value by applying the following equation:

$$R = \text{p}.\ L/A \tag{3.17}$$

where p is the resistivity of the module, which means that $\text{p} = \text{p}_n = \text{p}_p = 1.447 \times 10{-}5\ \Omega.\text{m}$, L is the thickness of the module (3.75 mm), and A refers to the surface area of the module $(0.04 \times 0.04)\ m^2$. By substituting Equation 3.17 into Equation 3.16, we obtain the result of the source term for every specific temperature difference, and by substituting Equation 3.16 into Equation 3.11 with the constant properties of the module, we get:

$$\partial/\partial x(k.\partial T/\partial x) + \partial/\partial y(k.\partial T/\partial y) + \partial/\partial z(k.\partial T/\partial z) - [(S^2.\Delta T^2/4R)\ /\ \forall] = 0 \tag{3.18}$$

Utilizing the CFD, the mean temperature difference across both sides of the TEG is determined, and then the maximum power generation is calculated by using the aforementioned temperature difference manually. Thereafter, it is assumed that the lateral surfaces of the thermoelectric module are adiabatic, therefore it is logical to

suppose that the heat just transfers in the x-direction, which is across the hot and cold surfaces of the thermoelectric module, as in the following equation:

$$d^2T/dx^2 + \dot{g}/k = 0 \tag{3.19}$$

By applying a double integral to Equation 3.19, it is possible to obtain the temperature value T(x):

$$T(x) = -(\dot{g}/2k).x^2 + C_1.x + C_2 \tag{3.20}$$

where $C_1$ and $C_2$ are constants as a result of the integration operation, and are found by substituting the value of (x) as the thickness or height of the module since for the hot side, x = 0, and for the cold side, x = 3.75 mm.

The heat fluxes of thermoelectric surfaces which are produced by flue gas in the hot channel, and which are produced by cooling water in the cold channel, can be represented thus:

$$\dot{q}_{s,h} = -\, k_{TE}.\, (dT_{s,h}/dx) \tag{3.21}$$

$$\dot{q}_{s,c} = -\, k_{TE}.\, (dT_{s,c}/dx) \tag{3.22}$$

Therefore, the output power of the thermoelectric module is:

$$\text{Output power } (P_{out}) = (\dot{q}_{s,h} - \dot{q}_{s,c}) \times A_{TEG} \tag{3.23}$$

The conversion efficiency (η) is an essential index for converting heat energy into electrical energy in thermoelectricity. The equation of conversion efficiency can be written thus:

$$\eta\ (\%) = P/Q_{s,h} \times 100 = (\dot{q}_{s,h} - \dot{q}_{s,c})/\dot{q}_{s,h} \times 100 \tag{3.24}$$

where $Q_{s,h}$ is the total heat transfer rate from the hot fluid to the thermoelectric module, and the heat fluxes at the hot and cold surfaces, respectively, are denoted by $\dot{q}_{s,h}$ and $\dot{q}_{s,c}$.

## 3.3. NUMERICAL ANALYSIS

### 3.3.1. Numerical Analysis Stages

This study utilizes the commercial software ANSYS Fluent 2020R2 to simulate the heat transfer processes through a thermoelectric generator to achieve a waste heat recovery system. The numerical simulation contains five stages to accomplish numerical analysis for our models. These stages begin with the establishment of the geometry. In the first stage, DesignModeler software is used to create a compact three-dimensional model using creation and modifying tools accurately and assembling all bodies into one part. Shared topology is employed to obtain united nodes between the contact bodies for exact analysis, as shown in Figure 3.7.

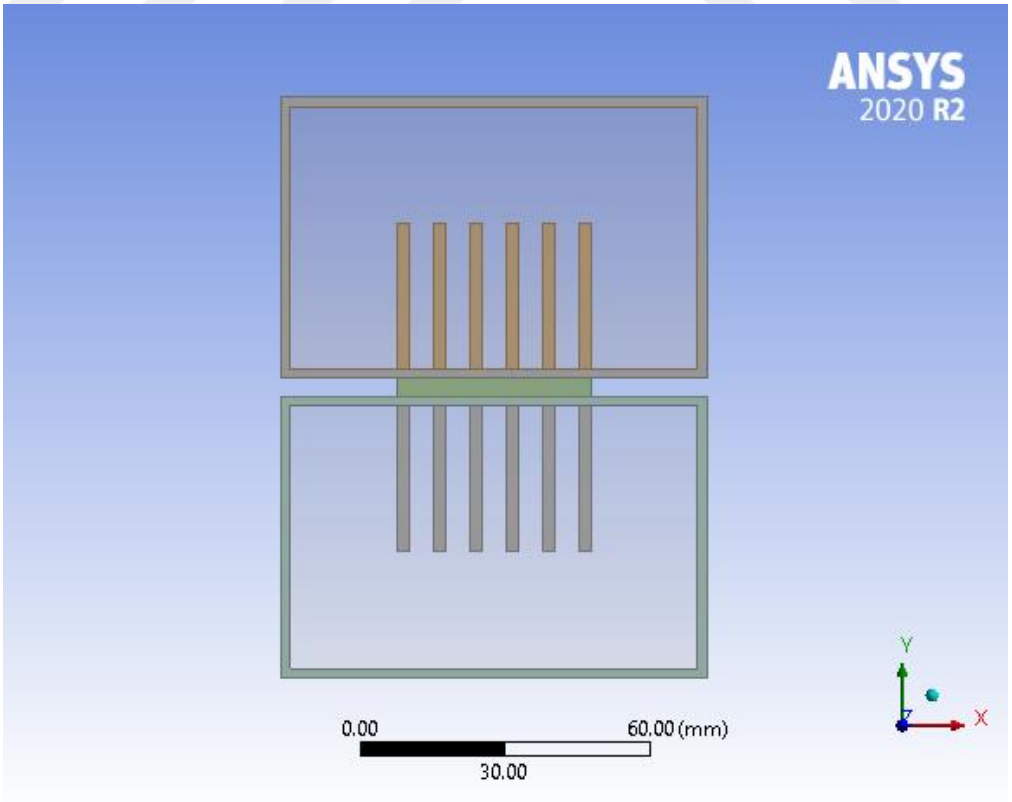


Figure 3.7. Three-dimensional model.

In the figure above, there are seven components prepared for the next stage. The components are two channels, two square pin fin heat sinks, the thermoelectric module and two flow domains. The upper domain is for cooling water and the lower for hot exhaust gas.

After exporting the geometry to ANSYS Mesh software, mesh generation becomes the second and more important stage. The software is utilized to create two-dimensional or three-dimensional grids, such that it divides complicated geometries into many elements and nodes in different shapes that are capable of discretizing a domain. One of the most important factors that should be taken into account to ensure simulation accuracy is creating a high-quality mesh. Engineering simulations need to begin with the best possible mesh because it affects the simulation in terms of results precision, iterations convergence and speed of performance. Mesh types are classified according to the geometry of the elements. For example, for a two-dimensional grid, a triangle (TRI) and quadrilateral (2D-prism) are used, while a tetrahedron (TET), hexahedron (HEX), pyramid, prism (wedge) and polyhedron are employed for a three-dimensional grid [42], as shown in Figure 3.8.

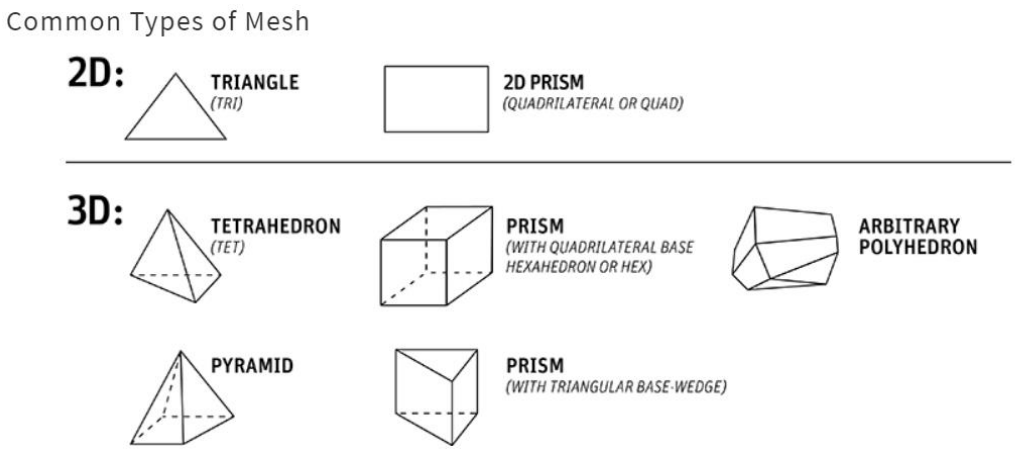


Figure 3.8. Common types of mesh.

In the current study, the basic aspects of a mesh are specified, since the physics and solver preferences are CFD and Fluent, respectively. Moreover, element order and size in general are linear and 3 mm. According to the sizing method, adaptive sizing is employed to make different sizes relevant. Body sizing methods are used, which gives

a different size for every domain and the size of bodies is specified according to the result of the grid independence test, as shown in Table 3.5.

Table 3.5. Element sizes for whole bodies.

| Body name | Element size (mm) |
|---|---|
| **Thermoelectric module** | 1.5 |
| **Hot and cold Heat Sinks** | 1.5 |
| **Hot and cold channels** | 1.2 |
| **Hot and cold flow domains** | 3.6 |

In our case, the internal flow of fluids produces boundary layers which are the extended layers between the wall and the point of free stream velocity that does not influence by the friction of the near-wall region. In turbulent flow, boundary layers divide into two main regions: inner and outer layers, as shown in Figure 3.9.

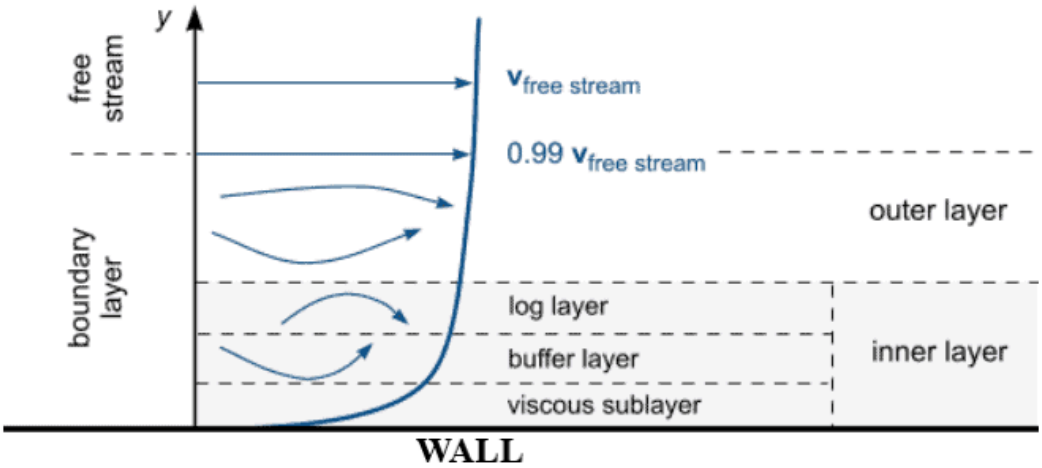


Figure 3.9. Boundary layers in turbulent flow.

The effective region is the inner layers that are divided into three divisions, these being a viscous sublayer, a buffer layer and a log layer. The importance of these layers comes from their near-to-wall boundary since a gradient of velocity or pressure occurs highly near to the wall region. Therefore, the elements layer should be computed accurately and an inflation layer for flow adjacent to the wall should be created. To achieve an accurate solution in the near wall region, we should use either the wall function method or resolve the viscous sublayer that depends on the $Y^+$ value [43], which means the dimensionless distance of the cell centroid to the adjacent wall is used to calculate the

height of the first layers. For a $Y^+$ value lower than 5, the solution of viscous sublayer can be used, but for a $Y^+$ value lower than 200 and higher than 30, the wall function method can be used. These limitations of $Y^+$ are indicated by previous experimental and theoretical studies [44], since the curve below Figure 3.10 indicates a similarity between experimental curves and CFD curves in the viscous sublayer and log layer regions, where the black curve is experimental. Blue and green curves are a result of CFD simulations. Therefore, we cannot use a $Y^+$ value higher than 5 and lower than 30 because there are no identical curves in the buffer layer.

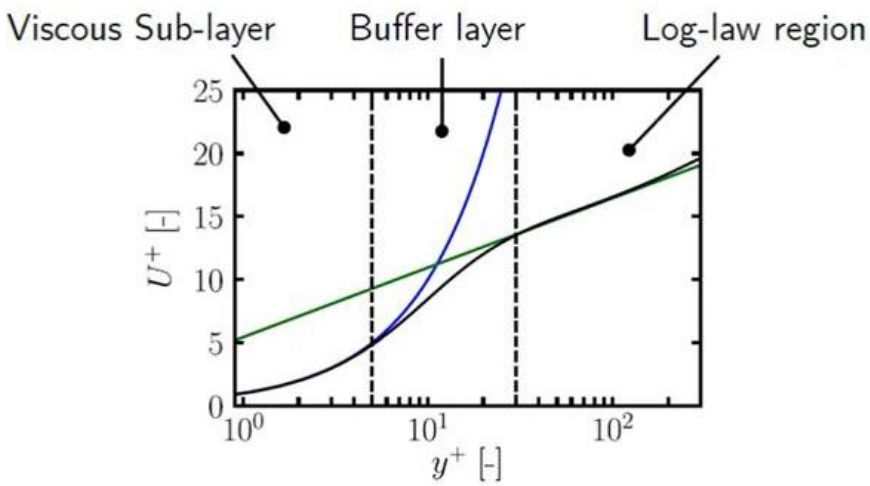


Figure 3.10. Difference between experimental and CFD curves.

Returning to our case, the study assumes a $Y^+$ value equal to 1 in order to resolve the problem in the viscous sublayer. Therefore, the first layer height is computed by following these steps:

- Start by calculating the flow Reynolds number (Re) from Equation 3.1.
- Use an empirical correlation for fully developed turbulent flow over a flat plate to estimate the skin friction coefficient ($C_f$):

$$C_f = [2\log_{10}(\mathrm{Re}) - 0.65]^{-2.3} \tag{3.25}$$

- After computing the skin friction coefficient, the wall shear stress ($\tau_w$) is calculated with the following equation:

$$\tau_w = 0.5.\rho U^2.C_f \tag{3.26}$$

- The friction velocity ($U_\tau$) can then be computed from the wall shear stress:

$$U_\tau = \sqrt{(\tau_w/\rho)} \tag{3.27}$$

- Equation of $y^+$ can be rearranged to give the height of the wall adjacent cell centroid from the wall ($y_p$) by assuming $y^+ = 1$.

$$y^+ = \frac{\rho . y_p . U_\tau}{\mu} \tag{3.28}$$

$$y_p = \frac{\rho . U_\tau}{\mu . y^+} \tag{3.29}$$

The total height of an element ($y_h$) equals double the $y_p$ value, as shown in Figure 3.11 below.

$$y_h = 2\ x\ y_p \tag{3.30}$$

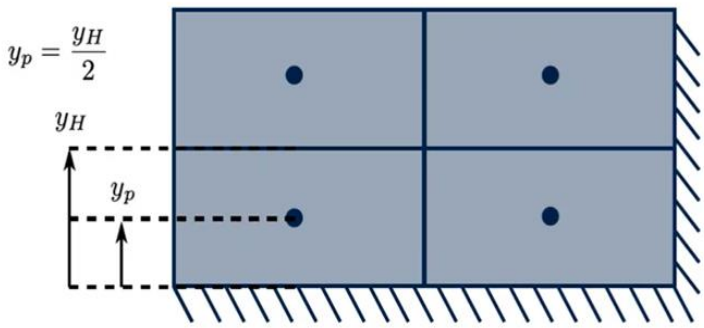


Figure 3.11. Height of the first layer.

When the aforementioned equations are applied, and when the Reynolds number equals 14,246 (9.59 m/s) of hot fluid flow, the results are $y_p = 0.08$ mm and $y_h = 0.16$ mm. Therefore, we create inflation layers around the hot and cold flow domains by using the first layer height equal to 0.16 mm and a growth rate of 1.2, as shown in Figures 3.12 and 3.13.

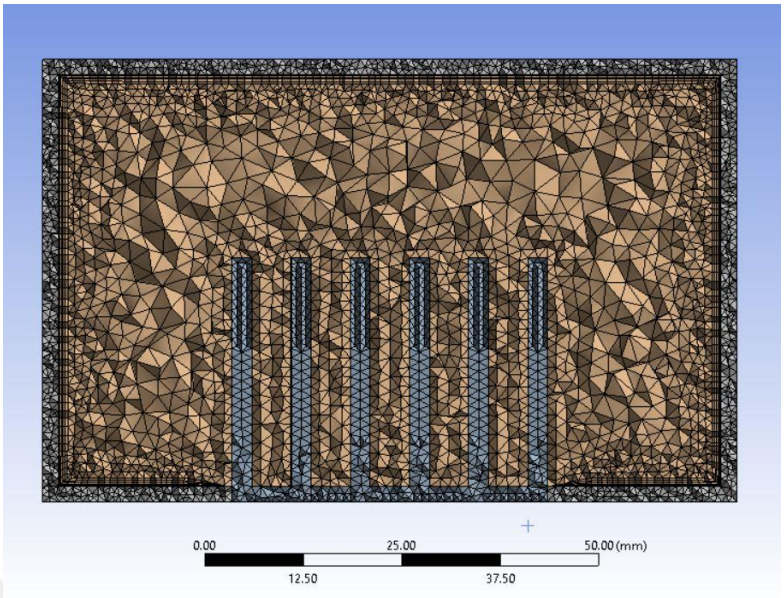


Figure 3.12. Cross-section of the meshed model.

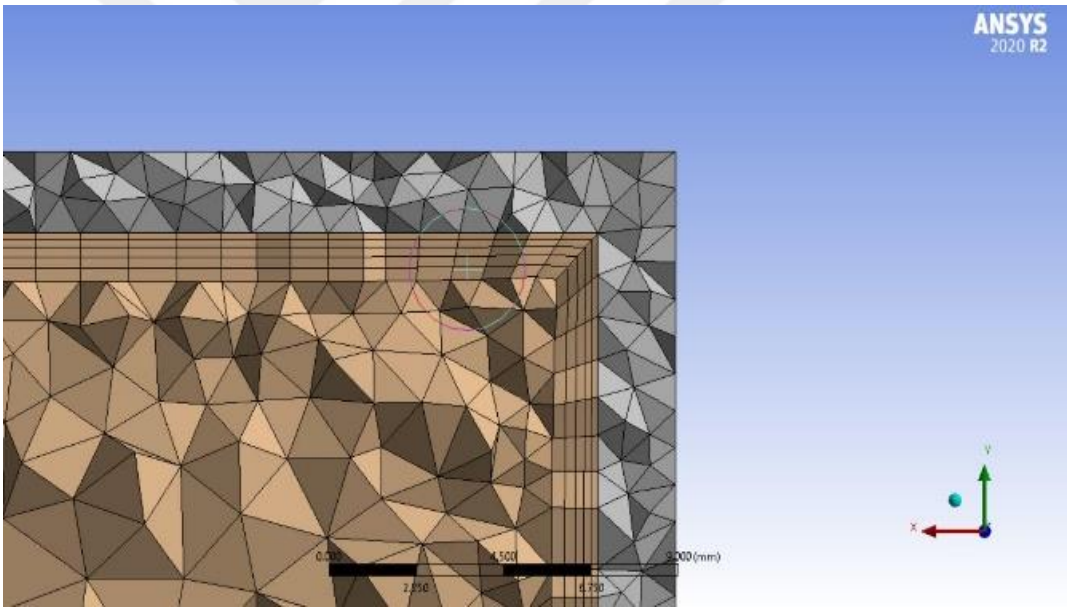


Figure 3.13. Illustration of inflation layers.

Finally, there are many parameters to measure the quality of a mesh, including aspect ratio, orthogonal quality, skewness and so on. All of these quality measurements are within acceptable limitations. Thereafter, the third stage is setup where a mathematical model of the solution is specified in addition to the boundary conditions and inlet parameters being employed. The solution stage is the fourth stage, which pertains to algorithm selection, and iteration accuracy and display results through the report

feature. The final stage is the results, which present the results of different parameters, such as velocity, pressure and temperature, as contours.

### 3.3.2. Numerical Method

The commercial software package ANSYS 2020R2 was employed to find solutions to the abovementioned equations by simulating the complete model of the waste heat recovery system. The SIMPLEC algorithm was specified to solve issues in terms of pressure-velocity coupling solutions [45]. The gradient of spatial discretization was based on the least square cell. The residual sum equation is:

$$\text{Residual sum} = \sum |a_{nb}\emptyset_{nb} + b - a_P\emptyset_P| \tag{3.31}$$

where $\emptyset$ is variable, a is coefficient and b represents the contribution of the constant portion of the source term ($\dot{g}$) [27]. The calculation approaches convergence and the iteration is finished whenever the sums of residuals are all less than $10^{-6}$ for continuity, energy, turbulent kinetic energy, and dissipation rate.

The simulation procedures consist of two sections. The purpose of the first simulation is to find the temperatures of the hot and cold sides of the thermoelectric module surface. The second simulation is utilized to discover all results, such as surfaces temperature, heat flux on surfaces and heat transfer rates.

During the first simulation, the appropriate turbulence model is chosen and the energy equation is checked, after which the properties of whole bodies, such as thermal conductivity, viscosity and specific heat, should be appointed. The inlet mass flow rates of hot and cold fluids are specified while the inlet temperatures of fluids are identified. The results of this simulation are the temperatures of the hot and cold sides of the thermoelectric module. Equations 3.1-3.6 are solved in this operation, after which we can obtain the temperature difference and substitute it into Equation 3.16 to find the source term ($\dot{g}$).

The steps of the second simulation are similar to the first, but we add the source term value into Equation 3.4 and follow by iteratively solving Equations 3.1 to 3.6 until the convergence conditions are met. By applying Equations 3.20-3.24, the researcher can obtain the temperature distribution on the thermoelectric module, heat flux on the module surfaces, output power and efficiency. Figure 3.14 shows the calculation procedures. Thermoelectricity and CFD are merged together to minimize computation time while maintaining accuracy.

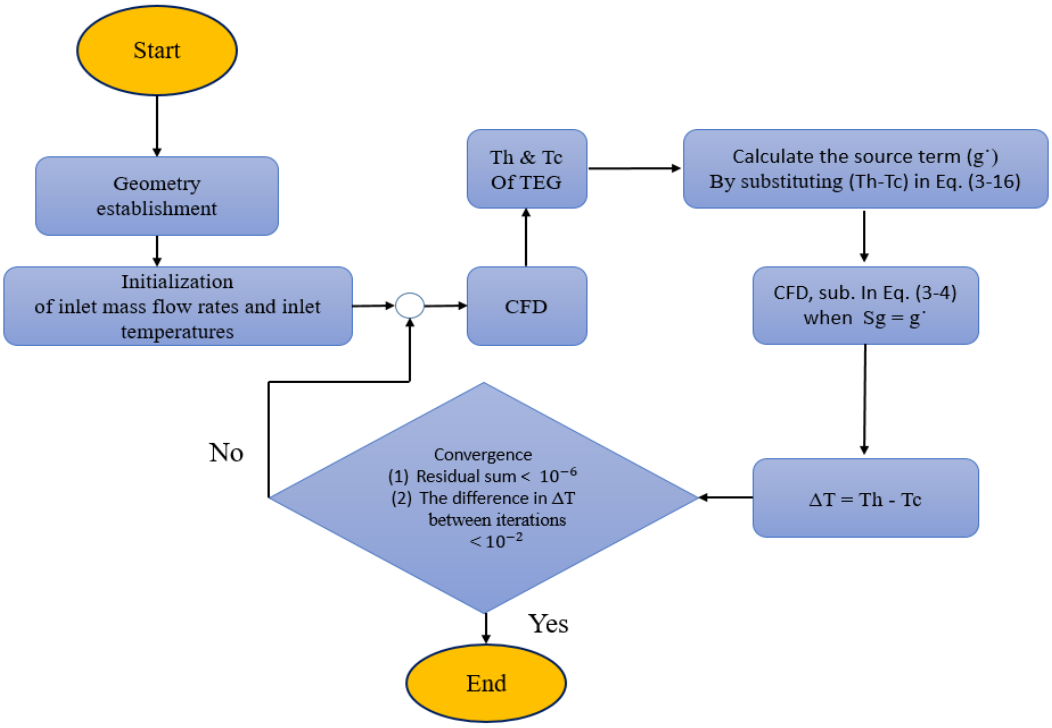


Figure 3.14. Flow chart of calculation procedures.

### 3.3.3. Turbulent Model Validation

To ensure the accuracy of the numerical analysis results, this study compares the current simulation results with previous simulation findings [14]. The same geometry is established by applying similar working conditions, and the flow is turbulent and at a steady state since the thermoelectric module is the same model. The validation case is carried out on the case which has the following working conditions: inlet mass flow rates of hot and cold fluids of 0.028 kg/s and 0.5 kg/s, respectively, and inlet temperatures of the hot and cold fluids of 603.15 K and 303.15 K, respectively. A

comparison between current and previous studies through the results reveals that the output power of this study equals 6.38 watts, while in the previous study it equals 6.12 watts. Therefore, the average relative error between the current study and the previous study is less than 5% in terms of output power according to the same turbulent model. Moreover, the result of the pressure drop is validated and gives an average relative error of 1.3% since the pressure drop of the current study is 13.03 Pa compared to the previous study value of 13.2 Pa.

### 3.3.4. Model Grid Independence

Grid independence is an important process in validating and verifying the accuracy of numerical simulations. This operation should occur before the prediction of the simulation to ensure exact results. This is accomplished by changing elements sizes thereby obtaining different grids which vary according to the elements number and keep the boundary conditions and constant parameters. The current study includes three different model configurations, the first of which includes hot and cold channels embedded into the two heat sinks of Model A, the second of which consists of hot and cold channels embedded into the two heat sinks of Model B, and the last of which is similar to the aforementioned two models but includes the two heat sinks of Model C. For the first model, five differently numbered grids are examined, these being 3,101,386, 3,305,927, 3,611,491, 4,516,085, and 5,970,642, as shown in Table 3.6. Five differently numbered grids for the second model are investigated, these being 3,246,110, 3,486,798, 3,769,342, 4,644,222, and 5,796,716, as shown in Table 3.7. For the third model, the numbers of grids are 2,699,324, 2,786,735, 3,215,315, 3,724,025, and 5,821,920, as shown in Table 3.8.

Table 3.6. Grid independence for the first model (A).

| No. | Number of elements | Number of nodes | Mesh element type |
|---|---|---|---|
| **1** | 3,101,386 | 792,309 | Tetrahedral and hexahedral |
| **2** | 3,305,927 | 837,256 | Tetrahedral and hexahedral |
| **3** | 3,611,491 | 913,640 | Tetrahedral and hexahedral |
| **4** | 4,516,085 | 1,122,264 | Tetrahedral and hexahedral |
| **5** | 5,970,642 | 1,441,002 | Tetrahedral and hexahedral |

Table 3.7. Grid independence for the second model (B).

| No. | Number of elements | Number of nodes | Mesh elements type |
|---|---|---|---|
| **1** | 3,246,110 | 816,010 | Tetrahedral and hexahedral |
| **2** | 3,486,798 | 869,342 | Tetrahedral and hexahedral |
| **3** | 3,769,342 | 939,488 | Tetrahedral and hexahedral |
| **4** | 4,644,222 | 1,143,694 | Tetrahedral and hexahedral |
| **5** | 5,796,716 | 1,409,419 | Tetrahedral and hexahedral |

Table 3.8. Grid independence for the third model (C).

| No. | Number of elements | Number of nodes | Mesh element type |
|---|---|---|---|
| **1** | 2,699,324 | 677,238 | Tetrahedral and hexahedral |
| **2** | 2,786,735 | 699,880 | Tetrahedral and hexahedral |
| **3** | 3,215,315 | 811,775 | Tetrahedral and hexahedral |
| **4** | 3,724,025 | 931,331 | Tetrahedral and hexahedral |
| **5** | 5,821,920 | 1,417,046 | Tetrahedral and hexahedral |

According to the requirement of less than 1% of relative errors when increasing or decreasing mesh element numbers to attain grid independence, the results of the temperature differences between the two surfaces for the first model in Figure 3.14 shows that the grid of 3,611,491 is implemented, while the results of the temperature difference between the two surfaces for the second model in Figure 3.15 show that the grid of 4,644,222 is utilized. In Figure 3.16, the third model reveals that the grid of 3,724,025 is appropriate for the numerical analysis. In conclusion, the objective of this operation was to assess whether the obtained solution is sufficiently accurate and provides us with the appropriate mesh structure that can be used to complete exact simulations.

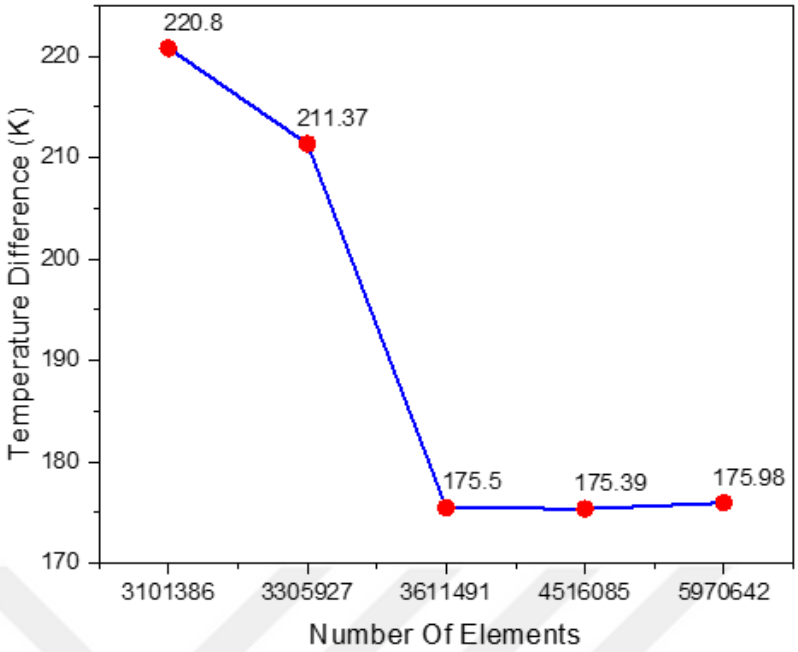


Figure 3.14. Temperature differences in the first model (A).

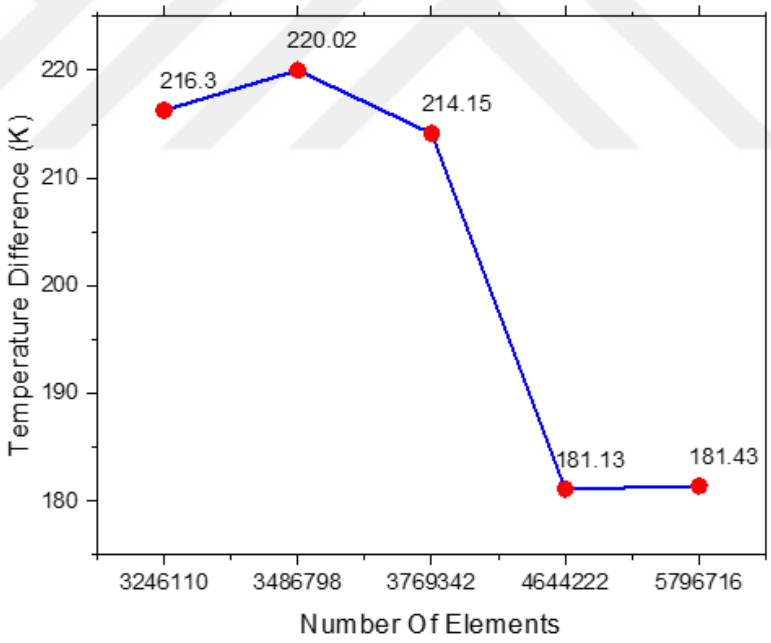


Figure 3.15. Temperature differences in the second model (B).

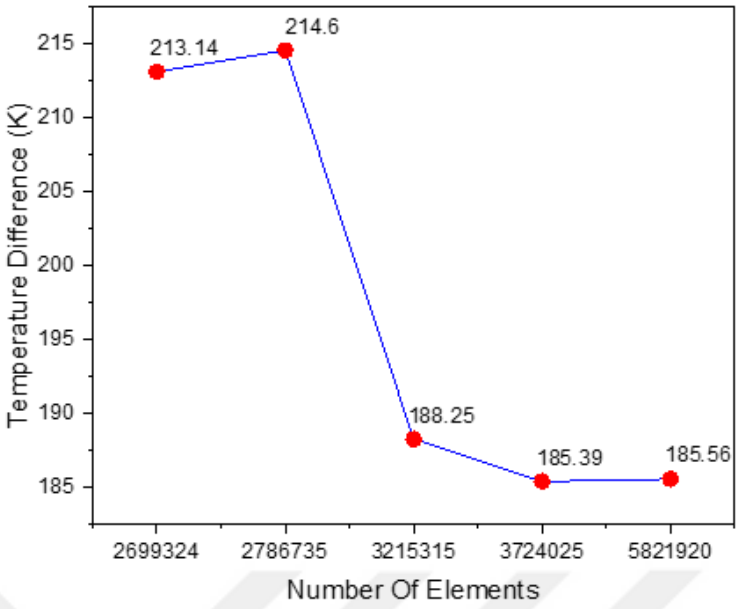


Figure 3.16. Temperature differences in the third model (C).

## 3.4. BOUNDARY CONDITIONS

In the current study, the exhaust gas is considered to be a hot fluid which flows through the hot channel, and the cooling water is proposed as a cold fluid to create a temperature difference through TEG surfaces. The flow of exhaust gas and cooling water is turbulent and at steady state since the Reynolds number of hot fluid is in the range of 4,457-14,264 in four different mass flow rates, as shown in Table 3.4, while the cold fluid remains at a constant mass flow rate with a Reynolds number of 7,197. The temperatures of the hot fluid are specified to be between 403.15 K and 553.15 K at four different temperatures, as shown in Table 3.3. The temperature of cold fluid, however, remains constant at 303.15 K. The walls of the channels are heat isolated (adiabatic wall), which means there is no heat flux around, and the lateral surfaces of the thermoelectric module are adiabatic. On the channel walls, no-slip boundary conditions are proposed, which means the velocity of fluids is zero. The outlets of both channels are postulated at one atmospheric pressure (1 atm). Finally, the heat transfer takes place on all contact surfaces between the channels, thereby inducing a temperature difference on the module surfaces.

# PART 4

# RESULTS AND DISCUSSION

The flow of hot and cold fluids was turbulent with four different mass flow rates for the hot fluid from 0.0088 kg/s to 0.028 kg/s, while the mass flow rate of the cold fluid was constant at 0.5 kg/s. The Reynolds number for the exhaust gas was in the range of 4,457-14,246, and at 7,197 for the cooling water. These mass flow rates were numerically investigated with four different temperatures between 403.15 K and 553.15 K using ANSYS Fluent 2020R2. The results of various simulations are presented in this part, including the effect of the hot fluid inlet temperature and influences of the temperature difference on the performance of the thermoelectric generating system in different models. Various heat transfer rates on the hot surface of thermoelectric module and their effect on performance were also investigated. The optimization of the pin size was investigated and achieved to produce three different models of heat sink to be embedded in channels. A comparison among these three models is presented and discussed in this part. For any findings of the numerical analysis, the output power and efficiency of the thermoelectric module were studied and illustrated using figures. In addition, the pressure drop and net output power for every model is investigated and discussed. This part includes interpretations and explanations for most of the following results of different cases as well as the illustration figures being used to clarify the cases.

## 4.1. TEMPERATURE DISTRIBUTION

In this study, the temperature of the cooling water was constant at 303.15 K, and the mass flow rate of water was constant at 0.5 kg/s. The temperature of the exhaust gas was specified within a range of 403.15 K to 553.15 K. It is extracted from automobile exhaust gas since at four hot fluid inlet temperatures of 403.15 K, 453.15 K, 503.15 K and 553.15 K with inlet mass flow rates of 0.0088 kg/s, 0.0146 kg/s, 0.0219 kg/s and

0.028 kg/s. Examinations of the hot fluid inlet temperatures and inlet mass flow rates were performed on Model C, where the size of the square pins of the heat sink are 2.5 mm × 2.5 mm × 30 mm numbering 78 pins. The results of these examinations showed that the optimal performance of the thermoelectric generating system occurs at an inlet temperature of 553.15 K and at an inlet mass flow rate of 0.028 kg/s, which is represented by a higher temperature difference (Figures 4.1 and 4.2).

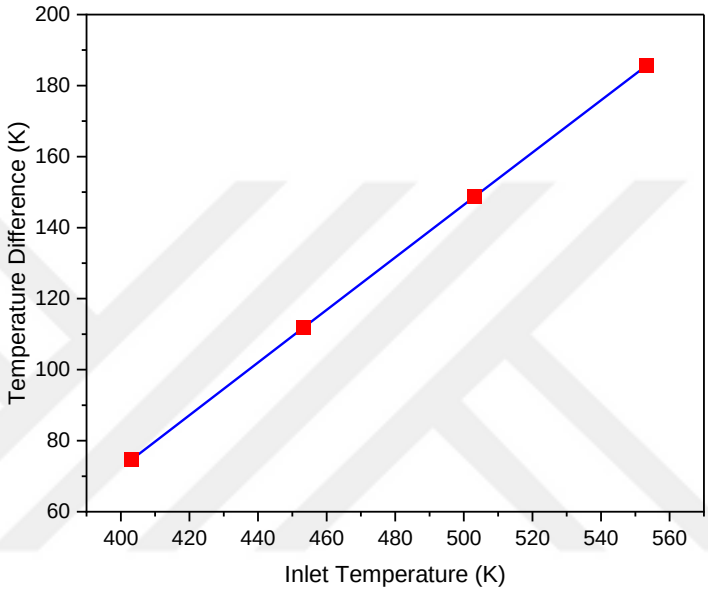


Figure 4.1. Relationship between inlet temperature and temperature difference.

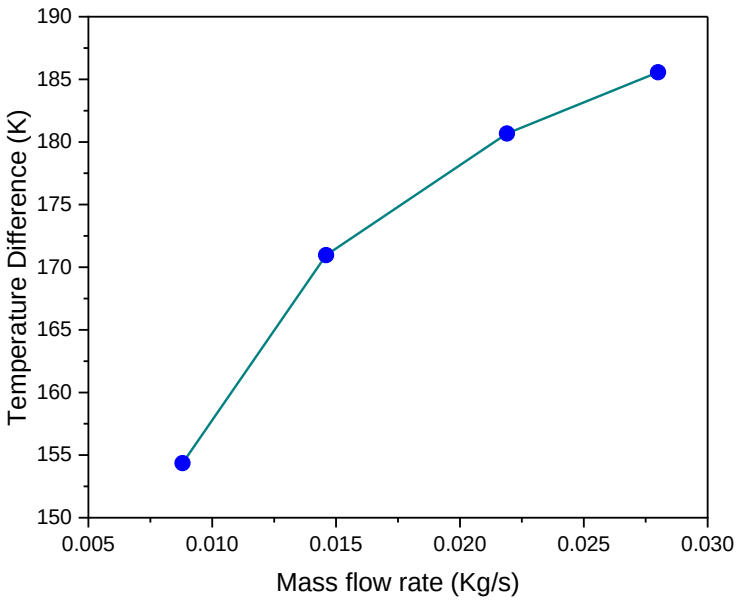


Figure 4.2. Relationship between inlet mass flow rate and temperature difference.

Figure 4.1 shows that the highest temperature of 553.15 K gives the optimal temperature difference of 185.56 K between two surfaces of the thermoelectric module, while Figure 4.2 shows that the inlet mass flow rate of 0.028 kg/s produces the same aforementioned temperature difference of 185.56 K. These parameters are used for the next comparison between heat sink models. In addition, the lower inlet temperature of 403.15 K with an optimal mass flow rate of 0.028 kg/s results in a lower temperature difference of 74.66 K, and a second inlet temperature of 453.15 K with an optimal mass flow rate of 0.028 kg/s induces a temperature difference of 111.77 K. The third inlet temperature with the same mass flow rate of 0.028 kg/s gives 148.74 K. The temperature difference occurs when the absorbed waste heat in the thermoelectric module is transferred to the cold surface of the module, then to the cold heat sink and cold fluid. The temperature difference is utilized by the thermoelectric module to achieve waste heat recovery and generate electrical power [46–48]. To understand the effects of the horizontal and vertical gaps between the square pin fins on the temperature distribution of the hot side of thermoelectric module and the surface area of the pins, three different isothermal contours are specified at the upper surface of the hot channel near the wall for each of the three models (A, B and C) of heatsink in our study, as shown in Figures 4.3., 4.4 and 4.5.

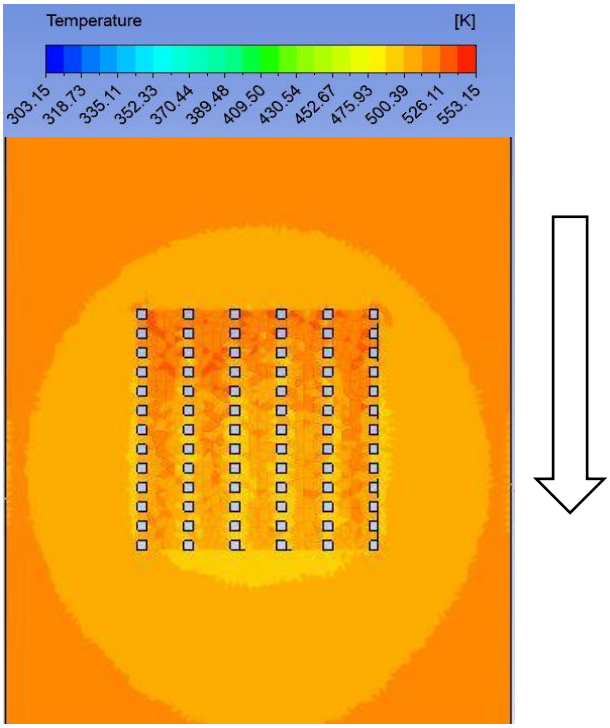


Figure 4.3. Isothermal contour for the upper surface of the hot channel in Model A.

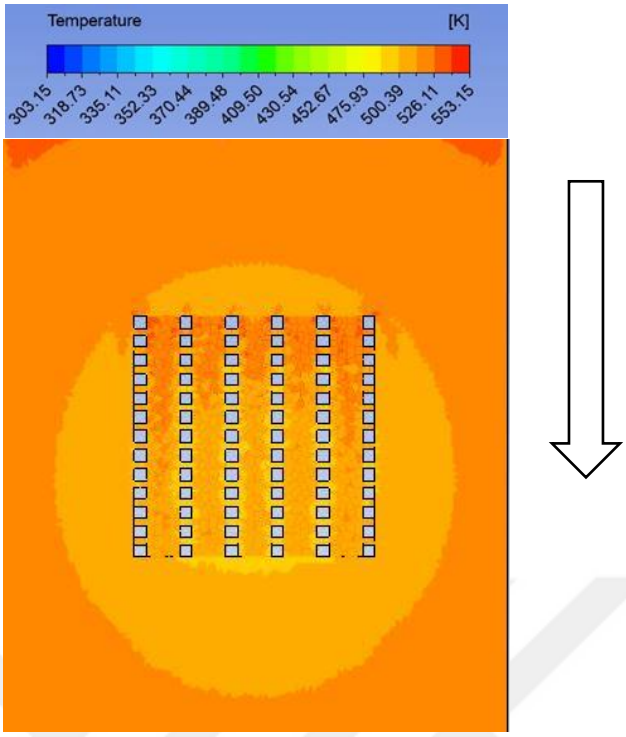


Figure 4.4. Isothermal contour for the upper surface of the hot channel in Model B.

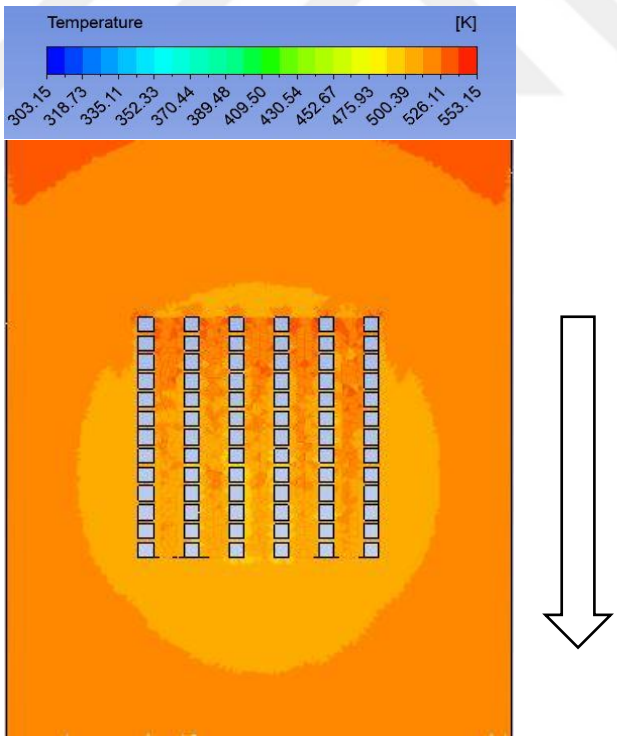


Figure 4.5. Isothermal contour for the upper surface of the hot channel in Model C.

It is observed that the temperature of the hot fluid drops precipitously during the hot fluid flow through the rows of pins since the fluid which passes through the first row

is thermally higher than the second row and other rows [27]. The isothermal contour of Model A in Figure 4.3 explains that the overall surface area of the square pins is smaller than Models B and C in Figures 4.4 and 4.5. The surface area of the square pins of Model A is 14,040 $mm^2$, 18,750 $mm^2$ for the square pins in Model B, and even larger for Model C at 23,400 $mm^2$. The optimal temperature differences of Models A, B and C are 175.98 K, 181.43 K and 185.56 K. The horizontal and vertical gaps (distances between fins) decrease when the temperature difference increases. This indicates that the heat exchange of Model A is lower than those of the other models. Moreover, the friction between the hot fluid and the square pins of Model A is lower compared to the other models during flow through the heat sink, which leads to fewer vortices and easier flow of the hot fluid indicating that the heat transfer is lower. We can deduct from these isothermal contours that the heat transfer performance increases when the surface area and cross-sectional area of square pins are increased [49]. The optimal isothermal contour is the Model C contour because of the greater surface area of the pins, the gaps are the smallest, and the friction is higher than other models' contours. The isothermal contours of the square pin fin heat sink in the hot side for each of the three models are shown in Figures 4.6, 4.7 and 4.8 below.

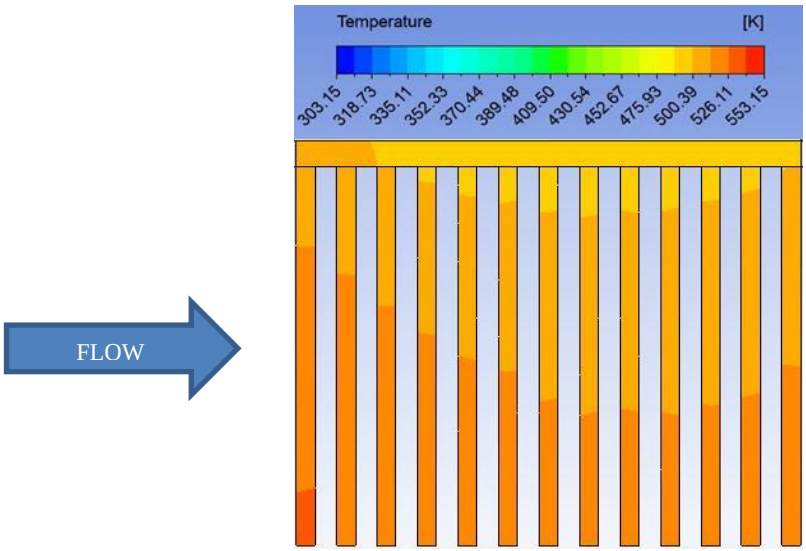


Figure 4.6. Isothermal contour of a square pin fin heat sink in Model A.

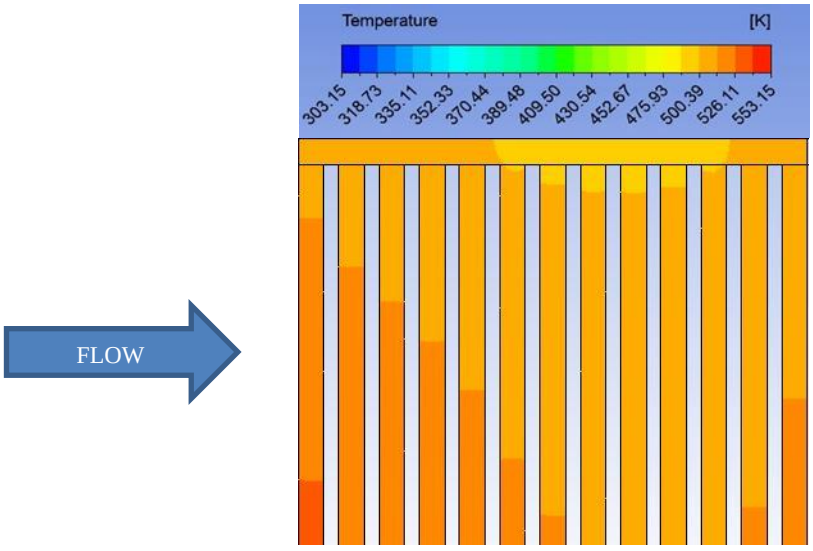


Figure 4.7. Isothermal contour of a square pin fin heat sink in Model B.

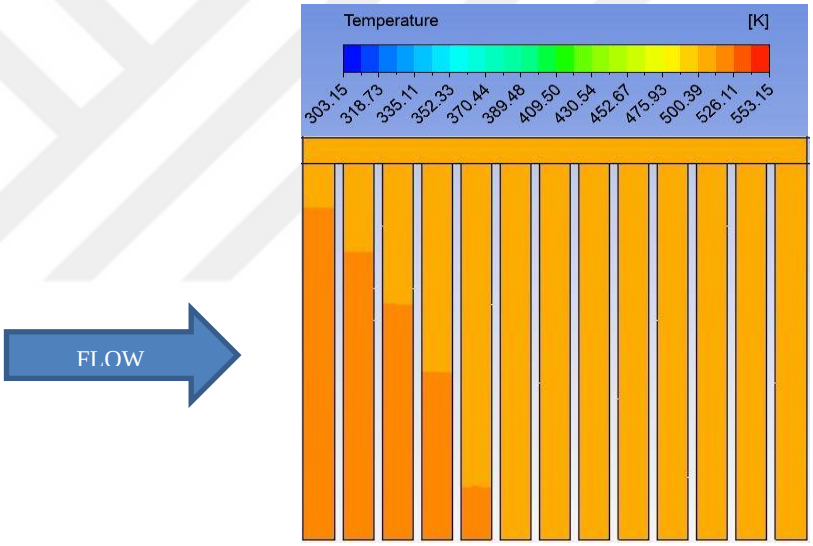


Figure 4.8. Isothermal contour of a square pin fin heat sink in Model C.

It is clear that the base of the heat sink in Model C has a higher temperature than the other models over a range of 500.39 K to 513.25 K, and that the temperature of square pins ranges from 500.39 K to 526.11 K. A temperature drop occurs from upstream to downstream, which usually means that the first row of pins absorbs more heat than the second, and the third row absorbs less than the second, and so on. This phenomenon has been mentioned by [50]. The temperature of the hot surface of the module is 497.45 K, while the base of the heat sink in Model B has a medium temperature over a range of 488.16 K to 513.25 K, which it is higher than the base temperature in Model A, which is also lower than the base temperature of Model C. The temperature

of the square pins ranges from 488.16 K to 526.11 K, but their surface area at a high temperature is less than that of Model C and more than that of Model A with consideration that the temperature of the hot surface of the thermoelectric module is 494.57 K. Moreover, the base of the heat sink in Model A has a temperature less than the other models between 475.93 K and 500.39 K. The temperature of the square pins ranges from 475.93 K to 539.63 K and their surface area at a high temperature is very small. However, the temperature of the hot surface of the module is 490.68 K. The temperature drop of the hot surface of the module for all models is logical and in a gradual manner, which supports the results for the cold surfaces of all the models where the temperatures of the cold surfaces of Models A, B and C are 314.71 K, 313.82 K and 311.89 K, respectively, according to the isothermal contours of the hot and cold surfaces of the thermoelectric modules each of the three models, as shown in Figures 4.9 and 4.10.

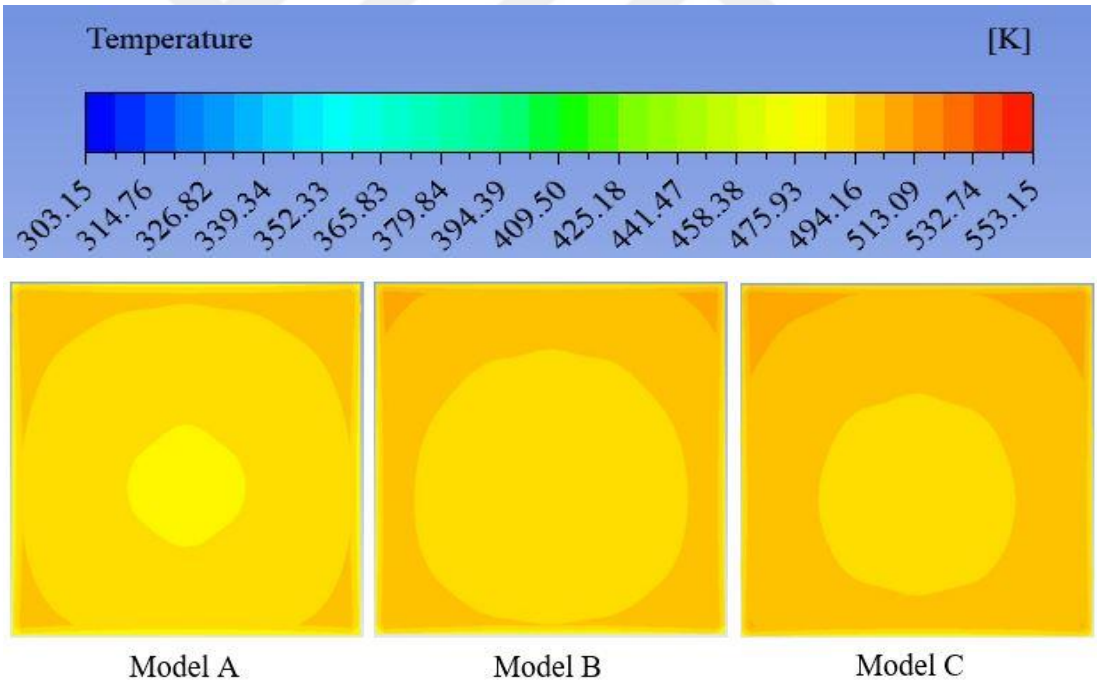


Figure 4.9. Isothermal contours of the hot surface of the TEG for the three models.

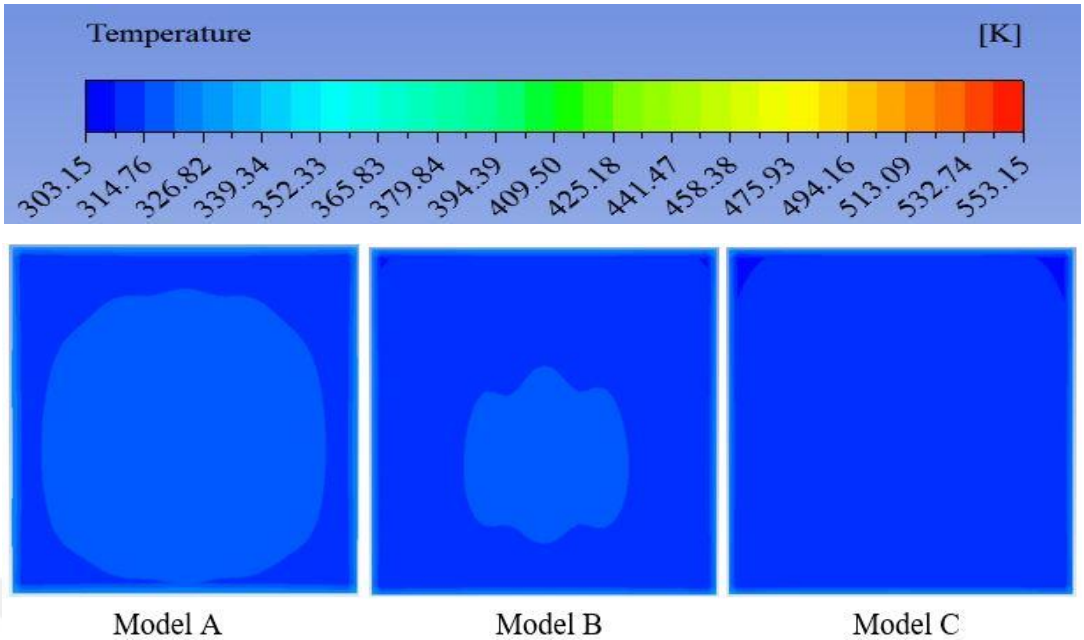


Figure 4.10. Isothermal contours of the cold surface of the TEG for the three models.

The reasons for the high temperatures of the cold surface in Model A is related to the smaller surface area which is exposed to the cooling fluid to cool the heat sink and the surface of the thermoelectric module. According to the findings of the temperatures of the hot and cold surfaces, the temperature difference of Model C is better than the other models. It is possible to generate a profile of temperature differences for comparison among all models, as shown in Figure 4.11.

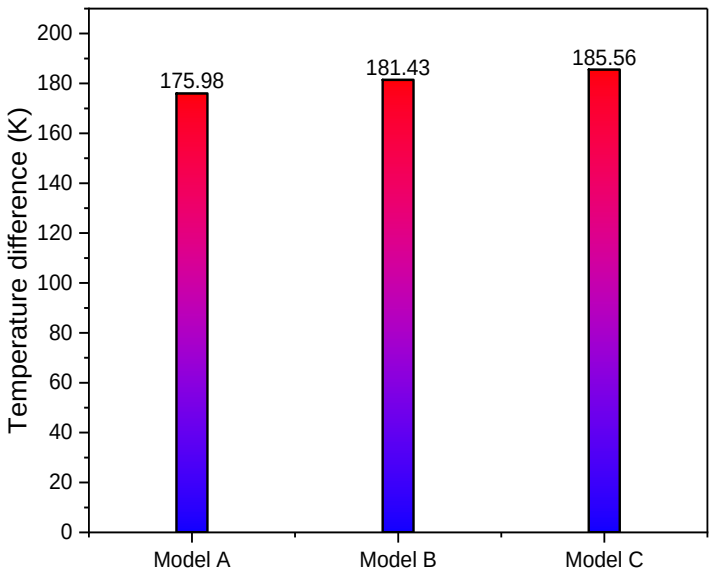


Figure 4.11. Comparison of the three models in terms of temperature differences.

## 4.2. HEAT TRANSFER RATE

Due to the isothermal contours as illustrated in Figures 4.3-4.8, heat transfer rates from the hot exhaust gas to the thermoelectric module are investigated. Here are two examinations, one for the temperature difference and the second for inlet mass flow rates being performed on Model C. When the temperature difference of 74.66 K and the mass flow rate of 0.028 kg/s are applied, the heat transfer rate is equivalent to 47.35 W. When the temperature difference of 111.77 K and mass flow rate of 0.028 kg/s are investigated, the heat transfer rate was found to be 70.1 W, and in the third case with a temperature difference of 148.74 K and mass flow rate of 0.028 kg/s, the heat transfer rate equals 92.2 W. In the last case when the temperature difference of 185.56 K and a mass flow rate of 0.028 kg/s are applied, the heat transfer rate is 113.69 W. In this examination, it can be concluded that the highest temperature difference with a constant mass flow rate gives the highest heat transfer rate on the hot surface of the thermoelectric module, as shown in Figure 4.12.

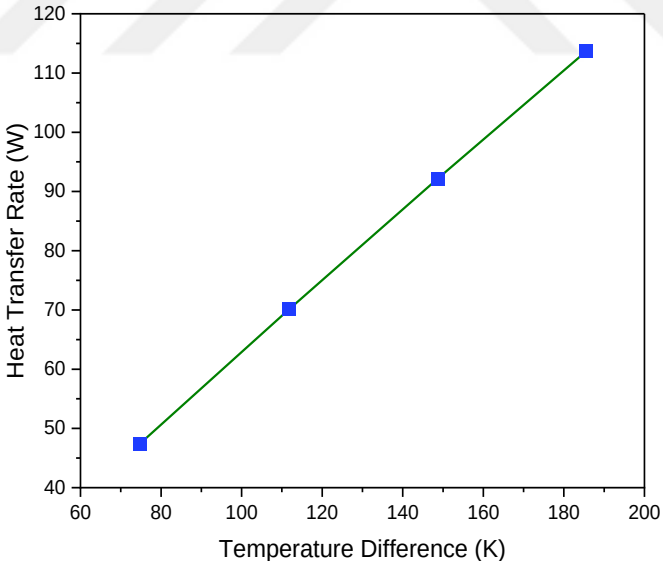


Figure 4.12. Relationship between temperature differences and heat transfer rates.

The second examination focused on the utilization of different inlet mass flow rates with a maximum inlet temperature of 553.15 K. A mass flow rate of 0.0088 kg/s results in a heat transfer rate of 95.24 W, and a mass flow rate of 0.0146 kg/s provides a heat transfer rate of 105.19 W. The heat transfer rate of 110.85 W is obtained by applying

a mass flow rate of 0.0219 kg/s, and a maximum mass flow rate of 0.028 kg/s achieves 113.69 W, as mentioned in the first examination, which means the maximum mass flow rate gives the highest heat transfer rate such as can be seen in the results of the examination of temperature differences, as shown in Figure 4.13.

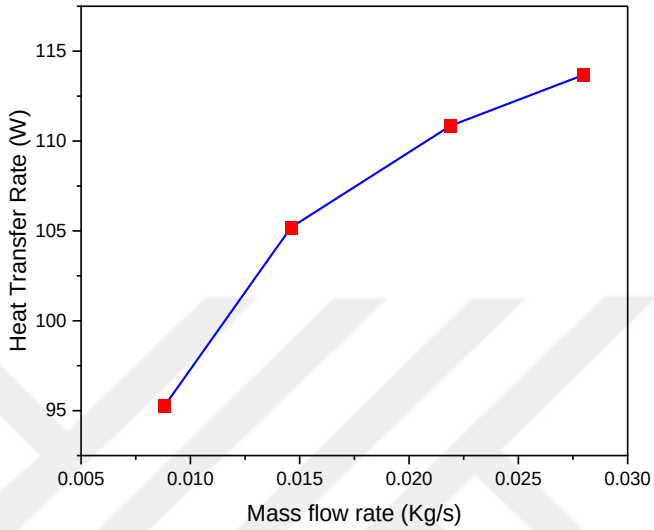


Figure 4.13. Relationship between mass flow rates and heat transfer rates.

The comparison among the three models is achieved in terms of heat transfer rates on the hot surface of the module and surface area when the highest inlet temperature of 553.15 K and maximum mass flow rate of 0.028 kg/s are applied, as shown in Figures 4.14 and 4.15. The heat transfer rate on the hot surface for Model C is 113.69 W, thereby making it 1.0214 fold the magnitude of the heat transfer rate of Model B, which in turn is 1.0513 fold that of Model A. However, the heat transfer rates of Models A and B are 108.14 W and 111.3 W, respectively. This confirms that the increase in pin size increases not only the surface area but also the turbulent flow and heat transfer coefficient and heat exchange performance [51]. Li et al. [52] investigated plate fins with different geometries and analyzed them thermally. The result showed that the larger fin surface area achieves greater thermal performance. This study ensures that the square pins of Model C possess a larger fin surface area and thus greater heat transfer performance.

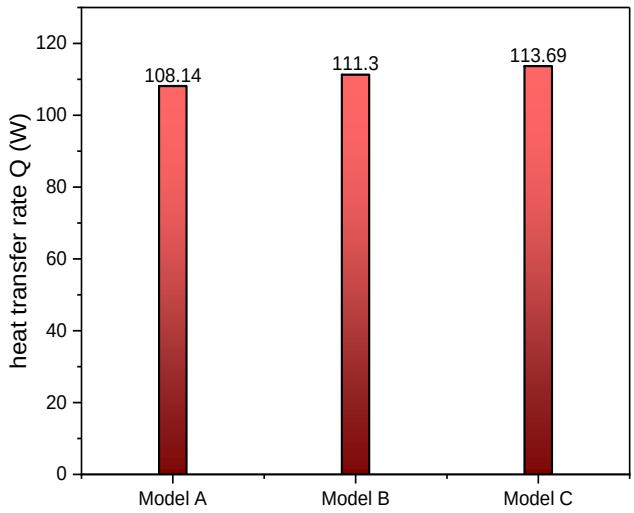


Figure 4.14. Comparison among the three models in terms of heat transfer rates.

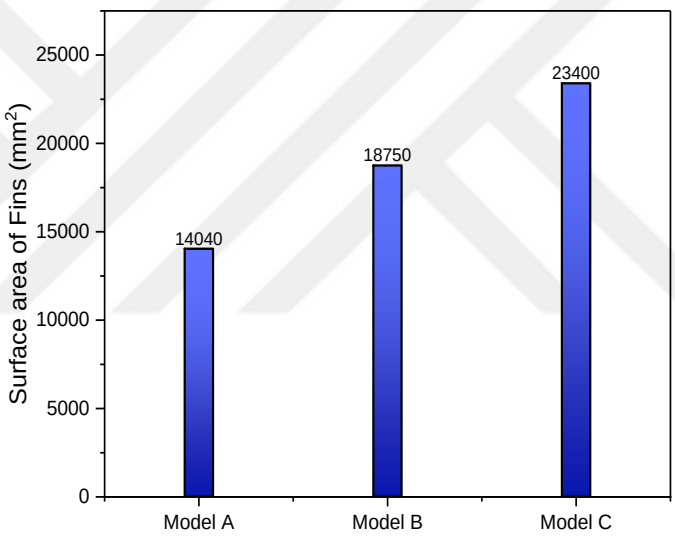


Figure 4.15. Comparison among the three models in terms of surface areas.

## 4.3. PERFORMANCE OF THE THERMOELECTRIC MODULE

Based on output power and efficiency Equations 3.23 and 3.24 in Part 3, it is necessary to obtain the net surface heat flux of the thermoelectric module for every numerical analysis from the results of the ANSYS software. Therefore, the net heat flux is presented for every examination in this section. The examinations are divided into two kinds, the first of which simulates various temperature differences with a constant inlet mass flow rate of 0.028 kg/s. These numerical analyses are performed on Model C. A temperature difference of 74.66 K and the aforementioned mass flow rate being applied produces a heat flux that is equivalent to 443.76 W/m$^2$. The output power and

efficiency of this analysis are 0.71 W and 1.5%, respectively. In the second case using a temperature difference of 111.77 K with the same mass flow rate, the results of the numerical analysis are 998.34 W/m$^2$. For the heat flux of the module's surfaces, moreover, 1.6 W and 2.28% are obtained as the output power and efficiency, respectively. By utilizing a temperature difference of 148.74 K under the same conditions above, the heat flux becomes 1,774.84 W/m$^2$, producing output power and efficiency of 2.84 W and 3.08%, respectively. The last case is when the temperature difference is 185.56 K with the same conditions, the heat flux of the module's surfaces is 2,773.17 W/m$^2$ respectively producing output power and efficiency of 4.44 W and 3.903%. The conclusion of the first examination indicates that as the heat flux and temperature differences increase, the output power and conversion efficiency also increase significantly, as shown in Figures 4.16 and 4.17.

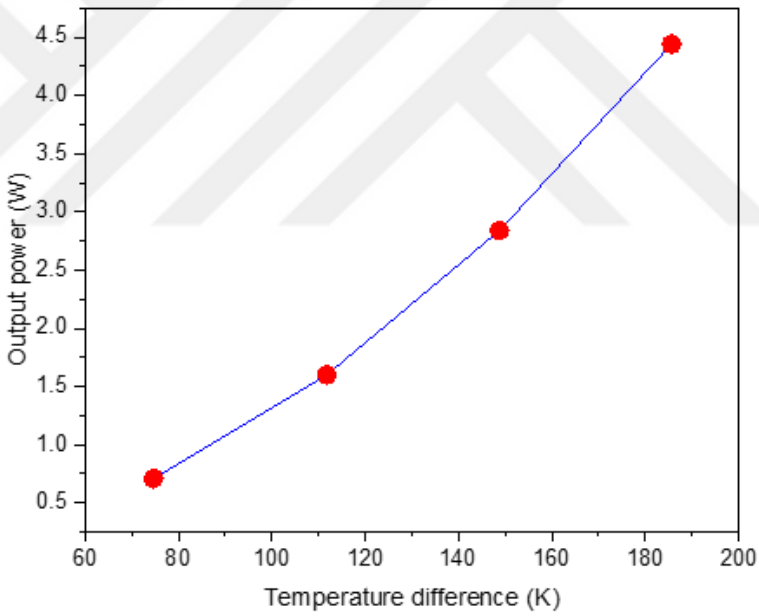


Figure 4.16. Relationship between temperature differences and output power.

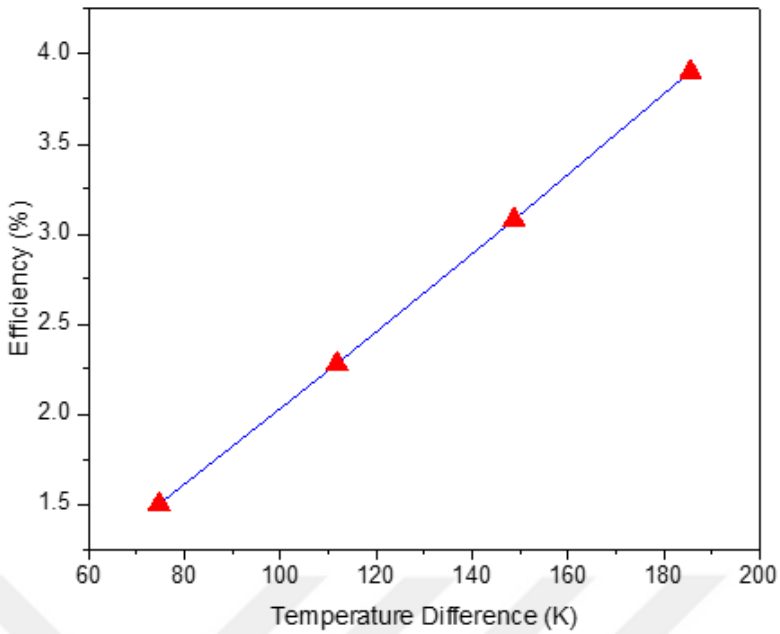


Figure 4.17. Relationship between temperature difference and efficiency.

The second examination simulates various inlet mass flow rates with a maximum inlet temperature of 553.15 K as a constant parameter. These numerical analyses are performed also on Model C. The mass flow rate of 0.0088 kg/s and the inlet temperature are applied, and the heat flux is equivalent to 2,026.79 W/m$^2$. As a result, the output power and efficiency of this analysis are 3.24 W and 3.405%, respectively. The second analysis is performed using the mass flow rate of 0.0146 kg/s with the same maximum temperature; the results of the numerical analysis would be 2,365.56 W/m$^2$ as the heat flux of the module's surfaces. Moreover, 3.79 W and 3.6% are obtained as the output power and efficiency, respectively. The third analysis is conducted utilizing a mass flow rate of 0.0219 kg/s and the same temperature as above; the heat flux, output power and efficiency were 2,633.44 W/m$^2$, 4.213 W and 3.801%, respectively. The last analysis is when the mass flow rate of 0.028 kg/s with the same conditions are used; the heat flux of the module's surfaces is 2,773.17 W/m$^2$, respectively giving the output power and efficiency as 4.44 W and 3.903%, as mentioned above in the first examination. Due to using the maximum temperature and a maximum inlet mass flow rate, the current study reveals that the inlet mass flow rates are directly proportional to the output power and efficiency of the thermoelectric module, as shown in Figures 4.18 and 4.19.

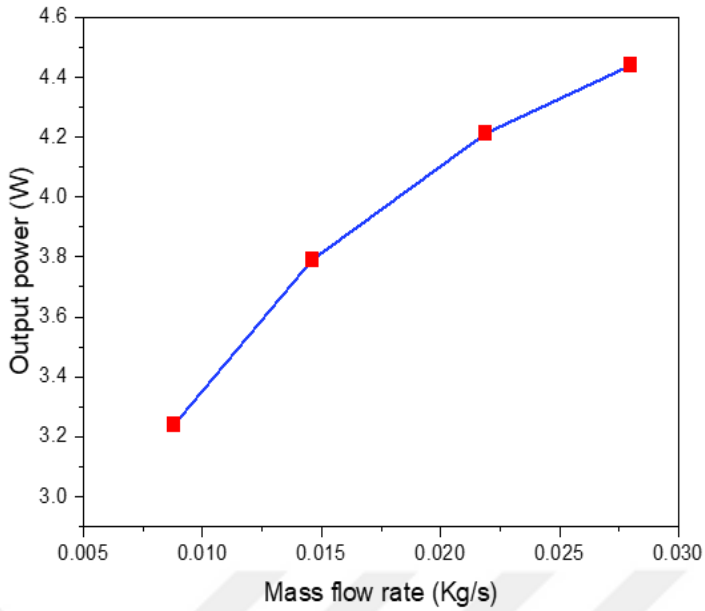


Figure 4.18. Relationship between mass flow rate and output power.

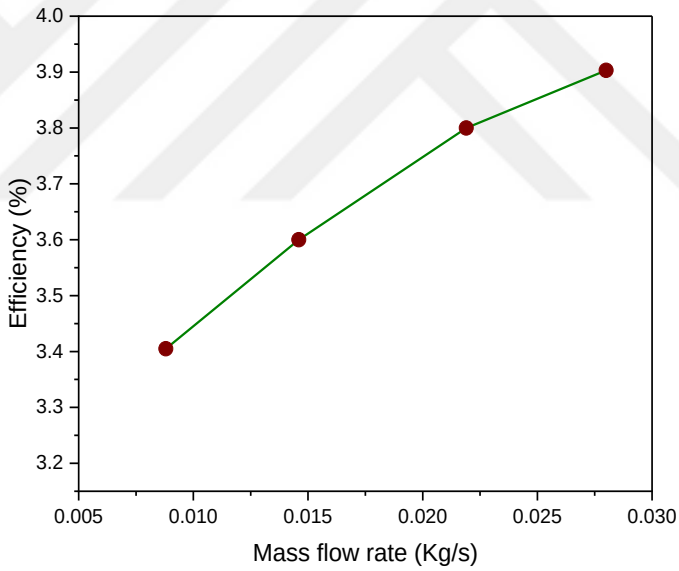


Figure 4.19. Relationship between mass flow rate and efficiency.

The comparison among the three models is carried out in terms of output power and efficiency of the thermoelectric module where the highest inlet temperature of 553.15 K and the maximum mass flow rate of 0.028 kg/s are applied, as shown in Figures 4.20 and 4.21. The output power and efficiency of thermoelectric module for Model C are 4.44 W and 3.903%, respectively, so the output power of Model C is 1.047 fold that of the output power of Model B, while it is 1.113 fold that of Model A. However, the output power and efficiency of Model B are 4.24 W and 3.81%, whereas

the least output power and least conversion efficiency are 3.99 W and 3.69%, respectively, for Model A. Finally, it is obvious that the output power and conversion efficiency are influenced by three factors: the size of the fins including their surface area and gaps, as well as the inlet parameters such as temperatures and mass flow rates. Therefore, the output power and conversion efficiency are improved when these three factors increase.

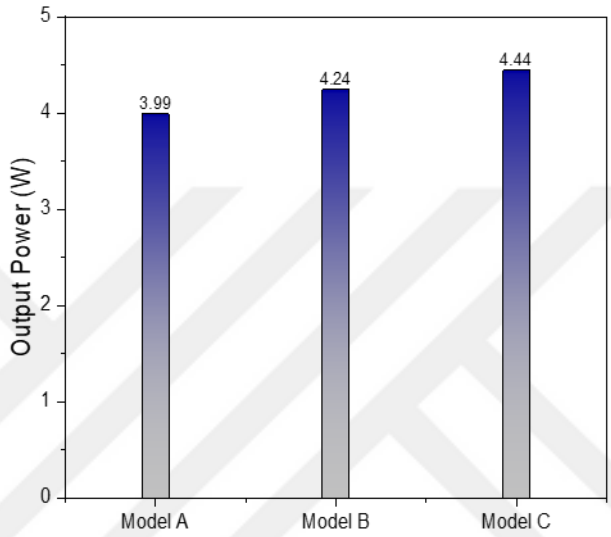


Figure 4.20. Comparison among the three models in terms of output power.

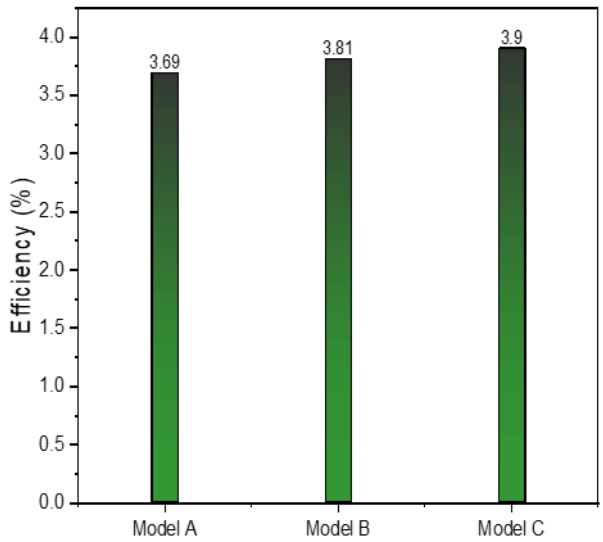


Figure 4.21. Comparison among the three models in terms of efficiency.

Due to our literature review, it is suitable to summarize the information and data related to thermoelectric generator systems according to parameters such as the type

of heat sink, the working fluid utilized in the study, the temperature differences which strongly affect the results, and the obtained maximum results from these studies, such as maximum output power and conversion efficiency. Table 4.1 shows how these data are classified.

Table 4.1. Different types of fins added to thermoelectric generator systems from the previous literature.

| Type of fins | Working fluid | Maximum power (W) | Maximum efficiency (%) | ΔT (K) | References |
|---|---|---|---|---|---|
| **Plate fins**<br>**Square pin fins** | HS: exhaust gas<br>CS: cold water | 4.93<br>6.12 | 5.74<br>6.42 | 134<br>145 | [14] |
| **Plate fins** | HS: wastewater<br>CS: cold water | 0.411 | 0.95 | ---- | [15] |
| **Plate fins** | HS: flue gas<br>CS: water | 2.70 | 3.50 | 151 | [27] |
| **Plate fins** | HS: waste gas<br>CS: water | 3.25 | ----- | 202 | [28] |
| **Plate fins** | HS: waste gas<br>CS: fixed temp. (363.15 K) | 1.33 | 3.23 | 310 | [29] |
| **Plate fins** | HS: exhaust gas<br>CS: water | 2.39 | ----- | 200 | [30] |
| **Plate fins** | HS: exhaust gas<br>CS: water | 13.08 | 2.58 | 282 | [31] |
| **Plate fins** | HS: exhaust gas<br>CS: water | 17.39 | ----- | 86 | [53] |
| **Square pin fins** | HS: exhaust gas<br>CS: water | 4.44 | 3.903 | 185.56 | This study |

HS and CS respectively denote the hot and cold states for hot and cold fluids.

## 4.4. EFFECT OF DIFFERENT TEMPERATURES UNDER THE VARIOUS MASS FLOW RATES

In general, the temperature range of exhaust gas is between 403.15 K and 553.15 K [53–55], and it is basically extracted from automotive exhaust gas under different engine conditions. Therefore, four different temperatures, of 403.15 K, 453.15 K, 503.15 K and 553.15 K, are taken into consideration in the numerical analysis when evaluating the effects of the hot fluid temperature on the heat transfer rate and thermoelectric performance for all cases. The effects of different temperatures under the various mass flow rates are investigated on the best performance model

(Model C). To investigate the effects of mass flow rate on the performance of a thermoelectric generating system, four mass flow rates of 0.0088 kg/s, 0.0146 kg/s, 0.0219 kg/s and 0.028 kg/s are used [56]. Figures 4.22 and 4.23 show the profiles of the heat transfer rate on the hot surface of the thermoelectric module and the temperature difference between the hot and cold surfaces of the module at different temperatures and mass flow rates. It is obvious that increase in the mass flow rate and inlet temperatures, whether together or individually, increases the temperature difference and heat transfer rate. The effect of inlet temperature is greater than the effect of inlet mass flow rates on the rate of heat transfer and temperature difference. For example, it is observed that an increase in inlet temperatures from 403.15 K to 553.15 K with a constant mass flow rate of 0.028 kg/s raises the heat transfer rate and temperature difference by less than 25 W and 40 K, respectively.

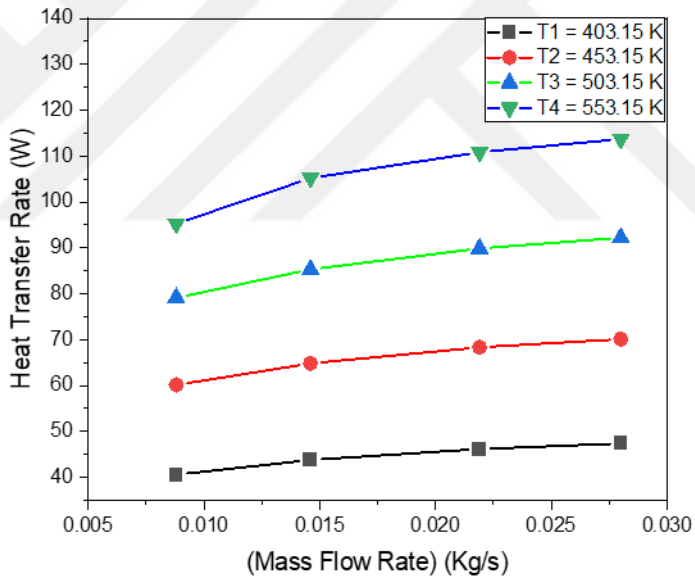


Figure 4.22. Comparison of heat transfer rate under different temperatures and different mass flow rate conditions.

The increase in mass flow rates from 0.0088 kg/s to 0.028 kg/s with a constant inlet temperature of 553.15 K increases the heat transfer rate and temperature difference in a range of 5 W to 10 W and 10 K.

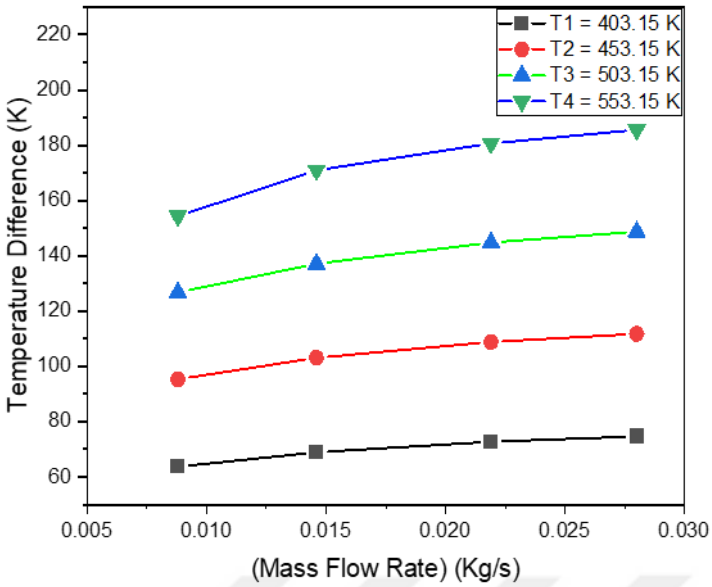


Figure 4.23. Comparisons of temperature differences under different temperatures and different mass flow rate conditions.

Figures 4.24 and 4.25 show the profiles of the thermoelectric module's output power and conversion efficiency. These profiles tend to be similar to the profiles of Figures 4.22 and 4.23. It has been noted that enhancing the temperature of the waste heat significantly improves output power and efficiency [31]. For instance, when the hot fluid inlet temperature increases from 403.15 K to 553.15 K with a constant inlet mass flow rate of 0.028 kg/s, the output power and conversion efficiency increase also from 0.71 W to 4.44 W and from 1.499% to 3.903%, respectively. Zhou et al. [54] investigated a novel structure, namely a cylindrical shell with plate fins for recovering waste heat from automobiles and explains the output power of a TEG at various inlet temperatures. Their findings revealed that the output power of the TEG increased by more than 40% when the inlet temperature increased by 100 K. This means that an increase in the inlet temperature of waste heat can effectively improve efficiency and increase output power. However, when the inlet temperature is constant and the mass flow rate increases from 0.0088 kg/s to 0.028 kg/s, the increase of output power and conversion efficiency is limited and insignificant.

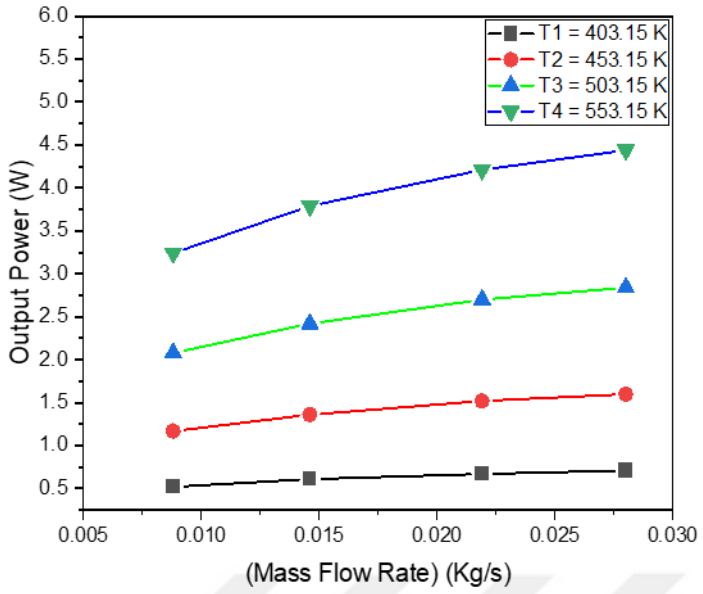


Figure 4.24. Comparisons of output power under different temperatures and different mass flow rate conditions.

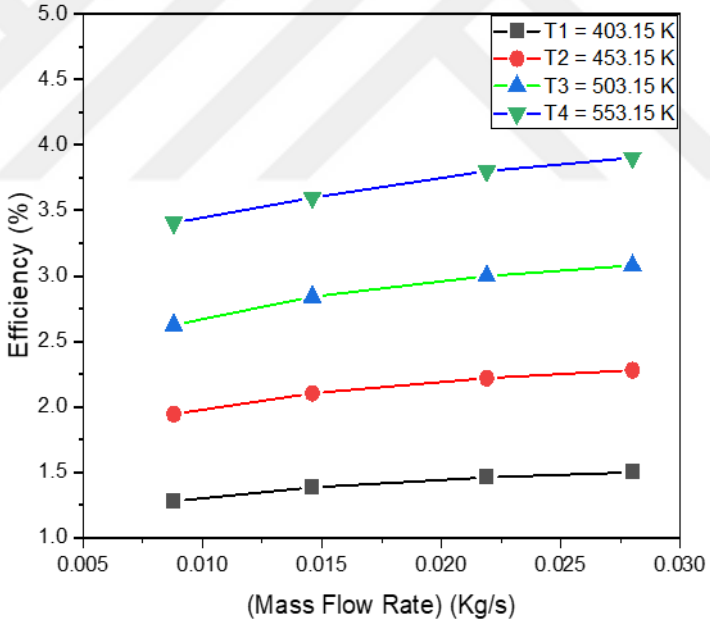


Figure 4.25. Comparisons of conversion efficiency under different temperatures and different mass flow rate conditions.

## 4.5. PRESSURE DROP AND NET OUTPUT POWER

In this study, the pressure drop is basically defined as the difference in pressure between the hot channel's inlet and outlet during the thermoelectric generating system. Moreover, it depends on several factors, such as mass flow rate, hot fluid viscosity,

channel roughness, hot fluid density and the length of the channel. Figure 4.26 shows the pressure drop in the hot channels for each of the three models. For Model A, it is 11.03 Pa, while for Model B, equaling 11.78 Pa. the magnitude of the pressure drop of Model B is higher than that of Model A. In addition, the pressure drop of Model C is higher than those of Models A and B at 13.07 Pa. The reasons for the increase in pressure drop gradually from Model A to Model C are the surface area of square pins and the overall pin size as mentioned previously. Model C possesses a larger surface area and volume of square pins than other models. This leads to effective flow separation around the pins, greater energy dissipation and a higher pressure drop [57].

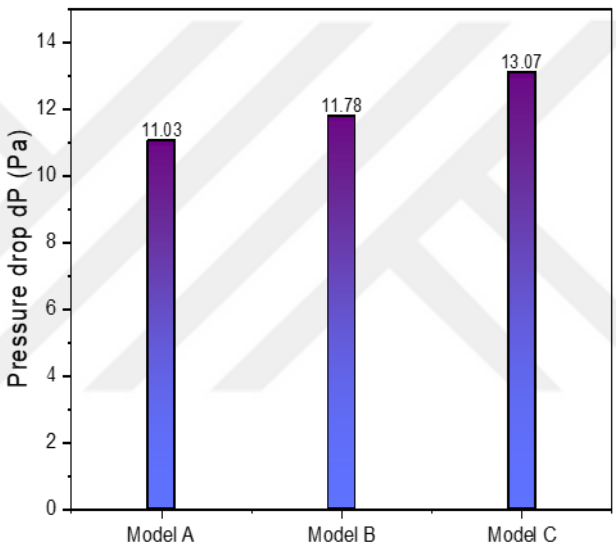


Figure 4.26. Comparison among the three models in terms of pressure drop.

The determination of net output power needs to obtain firstly the pumping power, which depends on volumetric or mass flow rate ($\dot{V}$) and pressure drop ($\Delta P$) for every model. Pumping power is calculated using the following equation [29]:

$$P_{Pump} = \dot{V}.\,\Delta P \tag{4.1}$$

where the pumping power of Models A, B and C are 0.31 W, 0.33 W and 0.37 W. It is possible to find the net output power by applying the following equation [50]:

$$P_{Net} = P_{Out} - P_{Pump} \tag{4.2}$$

where $P_{Out}$ is the output power of thermoelectric module, as mentioned in Figure 4.20. The net output power and output power profiles are illustrated in Figure 4.27. These are calculated from the above equations. This leads to the conclusion that when pressure drop increases, pumping power also rises, and the net output power thereafter decreases considerably.

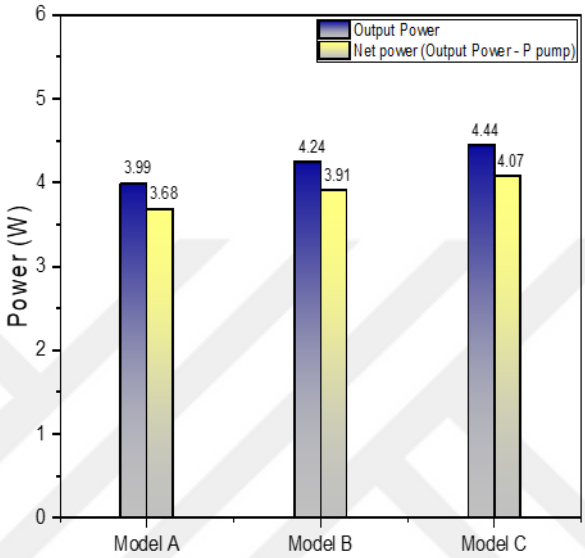


Figure 4.27. Comparison among the three models in terms of output power versus net output power.

# PART 5

## CONCLUSIONS AND SUGGESTIONS

In this part, the conclusions of the numerical analysis results of the different models are presented and the deductions of the various numerical simulations of different inlet parameters including a range of temperatures and mass flow rates for all models (A, B and C) are summarized as follows:

- The temperature difference increases by increasing the hot fluid inlet temperature with consideration of the constant mass flow rate for each model. Moreover, When the inlet mass flow rate is increased while maintaining the same temperature, the temperature difference rises. But the increase in temperature difference is less than that of the inlet temperature. The optimal inlet mass flow rate and optimal inlet temperatures respectively are 0.028 kg/s and 553.15 K. The best temperature difference is 185.56 K, which occurs in Model C.
- The investigation of the isothermal contours of a hot channel's top surface demonstrates that the heat transfer rates increase when the surface area of square pins increases. Vertical and horizontal gaps decrease when heat transfer rates increased. Model C achieves the best performance thermally such that the surface area of the square pins of Model C is 23,400 $mm^2$ and the vertical and horizontal gaps are 0.625 mm and 5 mm, respectively.
- The highest heat transfer rate on the thermoelectric module's hot surface is 113.69 W, which is obtained with a temperature difference of 185.56 K and a maximum mass flow rate of 0.028 kg/s, whereas the lowest heat transfer rate is 47.35 W, which is determined by applying a temperature difference of 74.66 K but the same mass flow rate of 0.028 kg/s. These results are taken from the numerical analysis on Model C. The heat transfer rates of all models are increased gradually from Model A to Model C. The rates are 108.14, 111.3

and 113.69 for Models A, B and C, respectively, under inlet temperature of 553.15 K and the maximum mass flow rate of 0.028 kg/s.

- The net surface heat flux of the thermoelectric module increases by increasing the temperature difference. Net surface heat flux is 2,773.17 W/m$^2$ when the temperature difference is 185.56 K, through analysis on Model C.
- The output power and conversion efficiency of the module are improved by increasing the temperature difference and heat flux. Highest output power and efficiency had been achieved during this study at 4.44 W and 3.903%, which were obtained from Model C, at a temperature difference of 185.56 K.
- A higher-pressure drop occurs with Model C, equivalent to 13.07 Pa, whereas the lowest pressure drop is 11.03 Pa in Model A. It was observed that by decreasing pumping power and pressure drop, the net output power increases. Models A, B, and C have a respective net output power of 3.68 W, 3.91 W, and 4.07 W.

The following are some suggestions for future studies to develop this study:

- Square pin fins can be tapered from different corners to conduct a comprehensive comparison.
- For cold fluid, it is possible to use various inlet temperatures and mass flow rates.
- The entire numerical analysis can be performed in laminar flow by utilizing low velocities.

## REFERENCES


1. E. Garofalo, M. Bevione, L. Cecchini, F. Mattiussi, and A. Chiolerio, “Waste Heat to Power: Technologies, Current Applications, and Future Potential,” ***Energy Technology***, vol. 8, no. 11. Wiley-VCH Verlag, Nov. 01, 2020. doi: 10.1002/ente.202000413.

2. Z. Su *et al.*, “Opportunities and strategies for multigrade waste heat utilization in various industries: A recent review,” ***Energy Conversion and Management***, vol. 229. Elsevier Ltd, Feb. 01, 2021. doi: 10.1016/j.enconman.2020.113769.

3. Mohsen, S., Hossein, M., and Sadeghzadeh, M., "Thermoelectric cooler and thermoelectric generator devices : A review of present and potential applications , modeling and materials", ***Energy***, 186: 115849 (2019).

4. He, W., Zhang, G., Zhang, X., Ji, J., Li, G., and Zhao, X., "Recent development and application of thermoelectric generator and cooler", ***Applied Energy***, 143: 1–25 (2015).

5. Zoui, M. A., Bentouba, S., Velauthapillai, D., Zioui, N., and Bourouis, M., "Design and characterization of a novel finned tubular thermoelectric generator for waste heat recovery", ***Energy***, 253: 124083 (2022).

6. Lingen, C., Fankai, M., and Fengrui, S. U. N., "Thermodynamic analyses and optimization for thermoelectric devices : The state of the arts", 59 (3): 442–455 (2016).

7. Maji, A., "Improvement of heat transfer through fins : A brief review of recent developments", (January): 1658–1685 (2020).

8. Yu, X., Feng, J., Feng, Q., and Wang, Q., "Development of a plate-pin fin heat sink and its performance comparisons with a plate fin heat sink", 25: 173–182 (2005).

9. Yang, Y. T. and Peng, H. Sen, "Numerical study of pin-fin heat sink with un-uniform fin height design", ***International Journal Of Heat And Mass Transfer***, 51 (19–20): 4788–4796 (2008).

10. Champier, D., "Thermoelectric generators : A review of applications", ***Energy Conversion And Management***, 140: 167–181 (2017).

11. Shen, Z., Tian, L., and Liu, X., "Automotive exhaust thermoelectric generators : Current status , challenges and future prospects", ***Energy Conversion And Management***, 195 (May): 1138–1173 (2019).

12. Oliver, J. and Malet, R., "Waste Heat Recovery Unit for Energy Intensive

Industries Thermoelectricity Harvesting", 423: .

13. Kaibe, H., Makino, K., Kajihara, T., Fujimoto, S., and Hachiuma, H., "Thermoelectric generating system attached to a carburizing furnace at Komatsu Ltd., Awazu Plant", ***AIP Conference Proceedings***, 1449 (April 2009): 524–527 (2012).

14. Chen, W. H., Wang, C. M., Huat Saw, L., Hoang, A. T., and Bandala, A. A., "Performance evaluation and improvement of thermoelectric generators (TEG): Fin installation and compromise optimization", ***Energy Conversion And Management***, 250 (October): 114858 (2021).

15. Chen, W. H., Chiou, Y. Bin, Chein, R. Y., Uan, J. Y., and Wang, X. D., "Power generation of thermoelectric generator with plate fins for recovering low-temperature waste heat", ***Applied Energy***, 306 (PA): 118012 (2022).

16. Liu, J., Shin, K. Y., and Kim, S. C., "Comparison and Parametric Analysis of Thermoelectric Generator System for Industrial Waste Heat Recovery with Three Types of Heat Sinks: Numerical Study", ***Energies***, 15 (17): (2022).

17. Şara, O. N., "Performance analysis of rectangular ducts with staggered square pin fins", ***Energy Conversion And Management***, 44 (11): 1787–1803 (2003).

18. Yang, K. S., Chu, W. H., Chen, I. Y., and Wang, C. C., "A comparative study of the airside performance of heat sinks having pin fin configurations", ***International Journal Of Heat And Mass Transfer***, 50 (23–24): 4661–4667 (2007).

19. Delfani, F., Rahbar, N., Aghanajafi, C., Heydari, A., and KhalesiDoost, A., "Utilization of thermoelectric technology in converting waste heat into electrical power required by an impressed current cathodic protection system", ***Applied Energy***, 302 (April): 117561 (2021).

20. Wang, C. C., Hung, C. I., and Chen, W. H., "Design of heat sink for improving the performance of thermoelectric generator using two-stage optimization", ***Energy***, 39 (1): 236–245 (2012).

21. Rezania, A. and Rosendahl, L. A., "A comparison of micro-structured flat-plate and cross-cut heat sinks for thermoelectric generation application", ***Energy Conversion And Management***, 101: 730–737 (2015).

22. Liu, J., Zhang, Y., Zhang, D., Jiao, S., Zhang, Z., and Zhou, Z., "Model development and performance evaluation of thermoelectric generator with radiative cooling heat sink", ***Energy Conversion And Management***, 216 (May): 112923 (2020).

23. Tzeng, S. C., Jeng, T. M., and Lin, Y. L., "Parametric study of heat-transfer design on the thermoelectric generator system", ***International Communications In Heat And Mass Transfer***, 52: 97–105 (2014).

24. Kim, D. K., Kim, S. J., and Bae, J. K., "Comparison of thermal performances

of plate-fin and pin-fin heat sinks subject to an impinging flow", ***International Journal Of Heat And Mass Transfer***, 52 (15–16): 3510–3517 (2009).

25. Chen, M., Rosendahl, L. A., and Condra, T., "A three-dimensional numerical model of thermoelectric generators in fluid power systems", ***International Journal Of Heat And Mass Transfer***, 54 (1–3): 345–355 (2011).

26. Chen, W. H., Wang, C. M., Lee, D. S., Kwon, E. E., Ashokkumar, V., and Culaba, A. B., "Optimization design by evolutionary computation for minimizing thermal stress of a thermoelectric generator with varied numbers of square pin fins", ***Applied Energy***, 314 (March): (2022).

27. Jang, J. Y., Tsai, Y. C., and Wu, C. W., "A study of 3-D numerical simulation and comparison with experimental results on turbulent flow of venting flue gas using thermoelectric generator modules and plate fin heat sink", ***Energy***, 53: 270–281 (2013).

28. Wan, Q. S., Liu, X., Gu, B., Bai, W. R., Su, C. Q., and Deng, Y. D., "Thermal and acoustic performance of an integrated automotive thermoelectric generation system", ***Applied Thermal Engineering***, 158 (April): (2019).

29. Ma, T., Lu, X., Pandit, J., Ekkad, S. V., Huxtable, S. T., Deshpande, S., and Wang, Q. wang, "Numerical study on thermoelectric – hydraulic performance of a thermoelectric power generator with a plate-fin heat exchanger with longitudinal vortex generators", ***Applied Energy***, 185: 1343–1354 (2017).

30. Luo, D., Wang, R., Yu, W., and Zhou, W., "A numerical study on the performance of a converging thermoelectric generator system used for waste heat recovery", ***Applied Energy***, 270 (May): 115181 (2020).

31. Cao, Q., Luan, W., and Wang, T., "Performance enhancement of heat pipes assisted thermoelectric generator for automobile exhaust heat recovery", ***Applied Thermal Engineering***, 130: 1472–1479 (2018).

32. Elankovan, R., Suresh, S., Karthick, K., Hussain, M. M. M. D., and Chandramohan, V. P., "Evaluation of thermoelectric power generated through waste heat recovery from long ducts and different thermal system configurations", ***Energy***, 185: 477–491 (2019).

33. Yazicioğlu, B. and Yüncü, H., "Optimum fin spacing of rectangular fins on a vertical base in free convection heat transfer", ***Heat And Mass Transfer/Waerme- Und Stoffuebertragung***, 44 (1): 11–21 (2007).

34. Ahsan, M., "Numerical analysis of friction factor for a fully developed turbulent flow using k–ε turbulence model with enhanced wall treatment", ***Beni-Suef University Journal Of Basic And Applied Sciences***, 3 (4): 269–277 (2014).

35. Maele, K. Van, Merci, B., and Dick, E., "COMPARATIVE STUDY OF k − ε TURBULENCE MODELS IN INERT AND REACTING SWIRLING FLOWS", (June): 1–10 (2003).

36. Turbulence, M., "Standard , RNG , and Realizable k - Models Theory Standard k - Model Overview Transport Equations for the Standard k - Model Modeling the Turbulent Viscosity", 12–26 (2006).

37. Chen, W., Lin, Y., Wang, X., and Lin, Y., "A comprehensive analysis of the performance of thermoelectric generators with constant and variable properties ☆", ***Applied Energy***, 241 (November 2018): 11–24 (2019).

38. Chen, W., Huang, S., Wang, X., Wu, P., and Lin, Y., "Performance of a thermoelectric generator intensi fi ed by temperature oscillation", ***Energy***, 133: 257–269 (2017).

39. Online, V. A., Yan, Y., and Malen, J. A., "Periodic heating amplifies the efficiency of thermoelectric energy conversion", 1267–1273 (2013).

40. Chen, W., Wu, P., Wang, X., and Lin, Y., "Power output and efficiency of a thermoelectric generator under temperature control", ***Energy Conversion And Management***, 127: 404–415 (2016).

41. Wang, Y., Shi, Y., Mei, D., and Chen, Z., "Wearable thermoelectric generator to harvest body heat for powering a miniaturized accelerometer", ***Applied Energy***, 215 (January): 690–698 (2018).

42. Canonsburg, T. D., "ANSYS Meshing User ' s Guide", 15317 (November): 724–746 (2010).

43. Salim, S. M. and Cheah, S. C., "Wall y + Strategy for Dealing with Wall-bounded Turbulent Flows", II: (2009).

44. Confidential, A., "Turbulence Modeling Introduction to ANSYS Fluent", (2014).

45. Taylor, P., Doormaal, J. P. Van, and Raithby, G. D., "Numerical Heat Transfer : An International Journal of Computation and Methodology ENHANCEMENTS OF THE SIMPLE METHOD FOR PREDICTING INCOMPRESSIBLE FLUID FLOWS", (February 2013): 37–41 (2007).

46. Wang, Y., Li, S., Xie, X., Deng, Y., Liu, X., and Su, C., "Performance evaluation of an automotive thermoelectric generator with inserted fi ns or dimpled-surface hot heat exchanger", ***Applied Energy***, 218 (February): 391–401 (2018).

47. Wang, Y., Li, S., Zhang, Y., Yang, X., Deng, Y., and Su, C., "The influence of inner topology of exhaust heat exchanger and thermoelectric module distribution on the performance of automotive thermoelectric generator", ***Energy Conversion And Management***, 126: 266–277 (2016).

48. Wang, Y., Wu, C., Tang, Z., Yang, X., Deng, Y., and Su, C., "Optimization of Fin Distribution to Improve the Temperature Uniformity of a Heat Exchanger in a Thermoelectric Generator", ***Journal Of Electronic Materials***, 44 (6): 1724–1732 (2015).

49. Mohankumar, D., Pazhaniappan, Y., and Ra, N. K., "Computational study of heat-transfer in extended surfaces with various geometries Computational study of heat-transfer in extended surfaces with various geometries", (2021).

50. Borcuch, M., Musiał, M., Gumuła, S., Sztekler, K., and Wojciechowski, K., "Analysis of the fins geometry of a hot-side heat exchanger on the performance parameters of a thermoelectric generation system", ***Applied Thermal Engineering***, 127: 1355–1363 (2017).

51. Guo, K., Zhang, N., and Smith, R., "Design optimisation of multi-stream plate fin heat exchangers with multiple fin types", ***Applied Thermal Engineering***, 131: 30–40 (2018).

52. Li, H. and Chao, S., "International Journal of Heat and Mass Transfer Measurement of performance of plate-fin heat sinks with cross flow cooling", ***International Journal Of Heat And Mass Transfer***, 52 (13–14): 2949–2955 (2009).

53. Liu, C., Deng, Y. D., Wang, X. Y., Liu, X., Wang, Y. P., and Su, C. Q., "Multi-objective optimization of heat exchanger in an automotive exhaust thermoelectric generator", 108: 916–926 (2016).

54. Zhou, M., He, Y., and Chen, Y., "A heat transfer numerical model for thermoelectric generator with cylindrical shell and straight fi ns under steady-state conditions", ***Applied Thermal Engineering***, 68 (1–2): 80–91 (2014).

55. Espinosa, N., Lazard, M., Aixala, L., and Scherrer, H., "Modeling a Thermoelectric Generator Applied to Diesel Automotive Heat Recovery", 39 (9): 1446–1455 (2010).

56. Yu, G., Shu, G., Tian, H., Wei, H., and Liu, L., "Simulation and thermodynamic analysis of a bottoming Organic Rankine Cycle ( ORC ) of diesel engine ( DE )", ***Energy***, 51: 281–290 (2013).

57. Taylor, P. and Catton, I., "Numerical Heat Transfer , Part A : Applications : An International Journal of Computation and Methodology Numerical Evaluation of Flow and Heat Transfer in Plate-Pin Fin Heat Sinks with Various Pin Cross-Sections", (November 2012): 37–41 .

## RESUME

Yasir Shakir ABDULSATTAR performed his first and elementary education in his city. He also completed a high school education in AL- Mutamayizeen High School, after that, he finished his bachelor study at University of Technology by graduating from Mechanical Engineering Department since 2012. Then in 2022, he started his postgraduate by studying at Karabuk University to complete M.Sc. education.